博　士　論　文

論文題目

Engineering photoswitching proteins for optogenetic control of cellular signaling processes

（細胞内シグナル伝達の光操作を実現する光スイッチタンパク質の開発）

氏名

河　野　風　雲

Engineering photoswitching proteins for optogenetic control of cellular signaling processes

A dissertation submitted to The University of Tokyo

for the degree of Doctor of Arts and Sciences

by Fuun KAWANO

Department of General Systems Studies

The University of Tokyo

Acknowledgements

The thesis is an assembly of results of my research at the Department of General Systems Studies, Graduate School of Arts and Sciences, The University of Tokyo, under the supervision of Professor Moritoshi Sato.

I wish to express my sincere gratitude to Prof. Moritoshi Sato for his continuous guidance, support, advice and encouragement throughput the present study. His essential questions and suggestions led me to think further and were indispensable in carrying out the present study.

I would like to express my deep gratitude to Dr. Hideyuki Suzuki, Graduate School of Arts and Sciences, The University of Tokyo, for his helpful suggestion and valuable discussion throughout this study. His adequate advice always led me to the right direction.

I really appreciate Mr. Yuki Aono, Graduate School of Arts and Sciences, The University of Tokyo, for considerable support in experiment, his stimulating discussion and continuous encouragement.

My special thanks are due to all the members of Prof. Moritoshi's laboratory for their stimulating discussion and continuous encouragement.

Finally, I would like to sincerely thank my family from the bottom of my heart for providing me with an opportunity to go to university and graduate school, and for supporting my school life.

Table of contents

Chapter 1

General introduction

1-1. To understand cellular signaling processes

Living organisms consist of a numerous number of living cells. In the case of *Homo sapiens*, they have more than 10^{13} cells that are classified into more than 200 cell types. These cells involve complex networks consisting of interactions among diverse biomolecules to respond to their environment by sensing intra- and extracellular signals and to translate the environmental cue into changes in gene expression and phenotypic alterations. The cellular networks are called signal transduction[1] (**Figure 1-1**). The dynamic nature of the all has been revealed by visualizing biomolecular activity and localization in real time with fluorescence imaging techniques[2]. In order to gain a deeper understanding of their roles in diverse cellular functions in the context of living cells at the molecular level, novel methods and technologies are required that allow optical control of biomolecule activities at a precise subcellular location and timing.

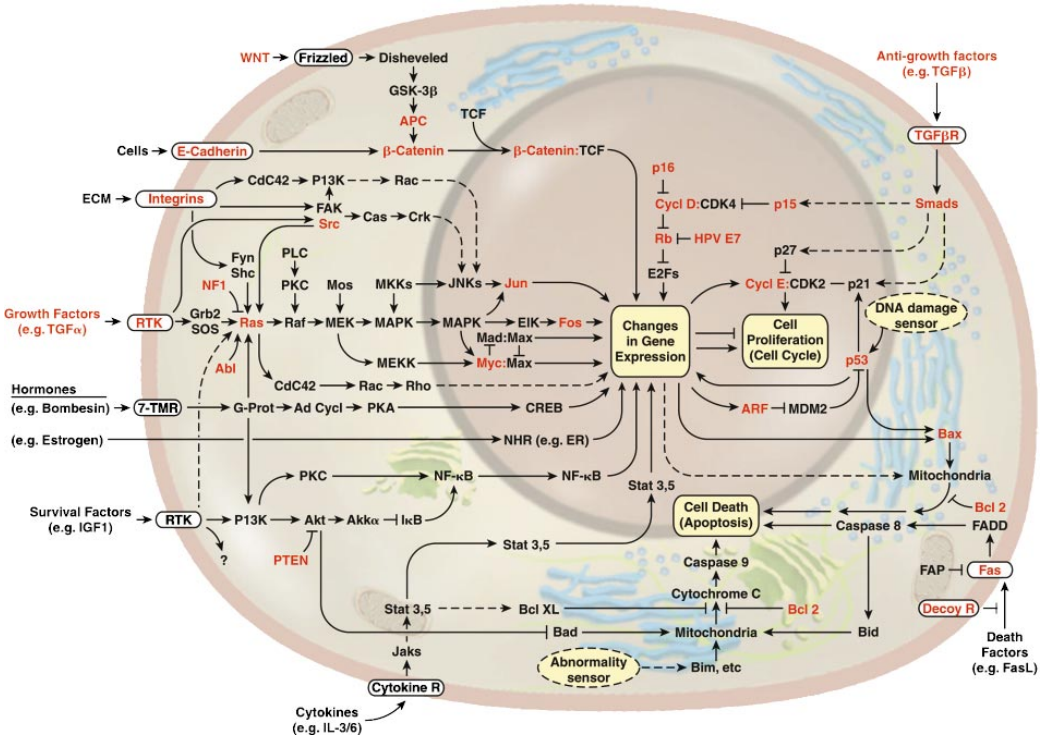

Figure 1-1. Overview of major signal transduction pathways.

1-2. Chemically inducible dimerization systems

The concept that two proteins are interacted only in the presence of a small molecule in living cells is first proposed and demonstrated in a landmark paper in 1993 by Spencer *et al*[3]. Thereafter, chemically inducible dimerization (CID) initiated by small molecules, called dimerizer, have been used as a tool for inducible and specific manipulation of a variety of signaling molecules in living cells and organisms[4-6]. The most commonly used chemical dimerizer is rapamycin, a macrolide immunosuppressant[7] (**Figure 1-2a**). The dimerizer induces interaction between FK506-binding protein (FKBP) and FKBP-rapamycin-binding protein (FRB)[7] (**Figure 1-2b**). Typical applications[4-6] using the CID system based on FKBP-rapamycin-FRB complex are shown in **Figure 1-3**. This principle has been used to manipulate various molecular processes, such as cellular signaling and gene expression, thereby resolving biological questions that were otherwise challenging. Recent efforts have been made to expand the palette of CID systems, aiming to control multiple signaling molecules at the same or different times and locations[3,7-11] (**Table 1-1**). CID systems have been shown to be powerful tools for the investigation of cellular events, however, spatial and temporal resolution of these methods are poor and they also lack tissue specificity.

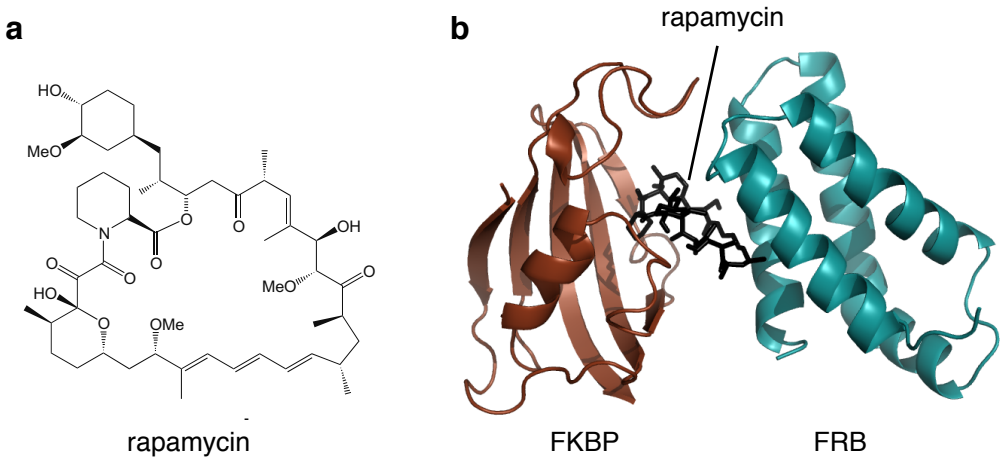

Figure 1-2. Structures of rapamycin (a) and FKBP-rapamycin-FRB complex (b).

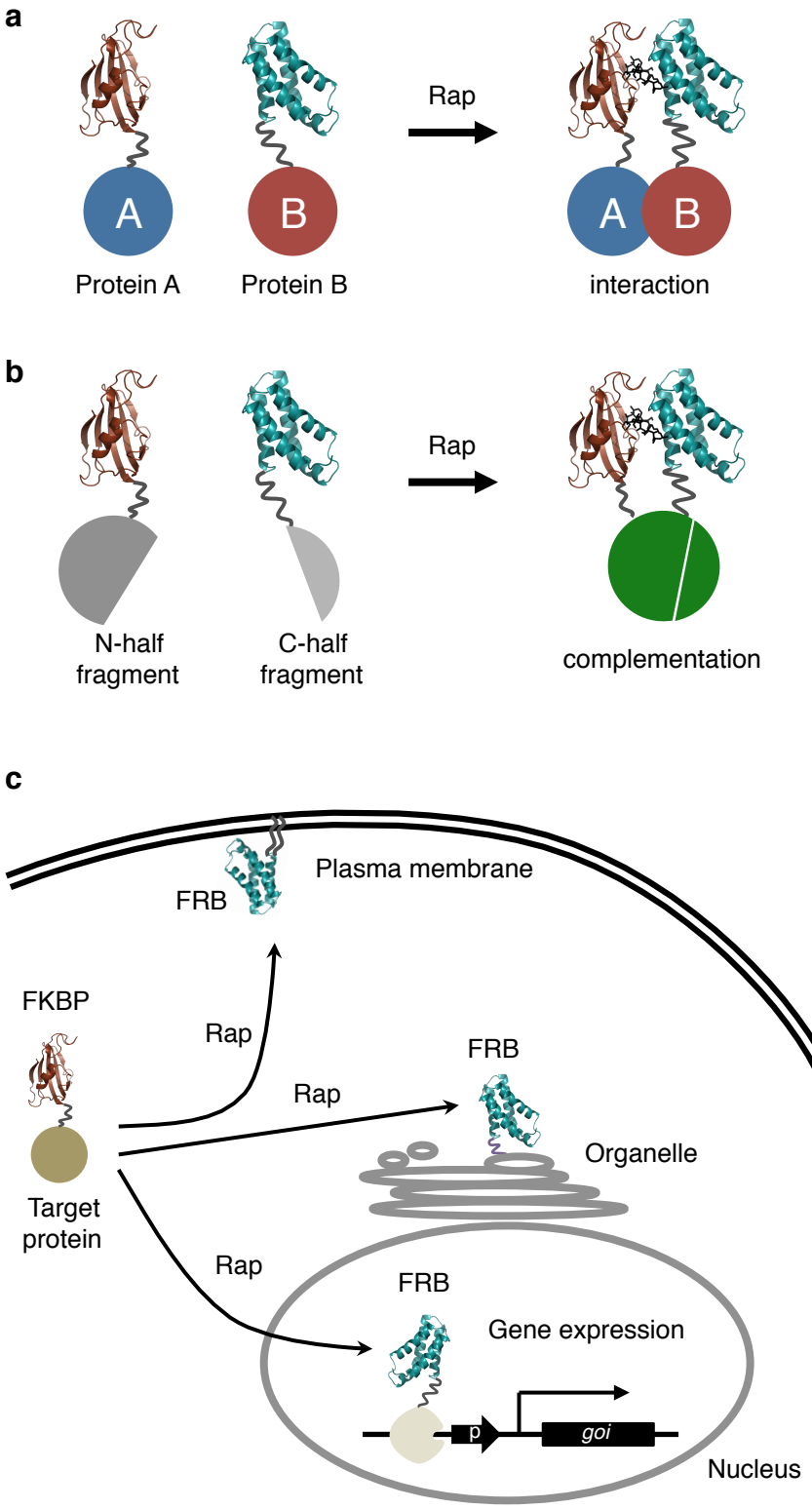

Figure 1-3. Applications of the CID system of ramamycin and FKBP-FRB for cellular proteins in living cells. (**a**) Rapamycin-dependent FKBP-FRB dimerization induces interaction between tagged protein A and protein B. (**b**) N-half fragment and C-half fragment of a split protein fused to FKBP and FRB are reconstituted by FKBP-rapamycin-FRB

complex. (**c**) Recruitment of a target protein tagged with FKBP to FRB anchored to various cellular locations, such as plasma membrane, organelle and nucleus.

Table 1-1. Variation of chemically inducible dimerization systems.

Dimerization component		Dimerizer	Reference
FKBP	FKBP	FK1012	[3]
FKBP	CAN	FK506	[8]
FKBP	CyP-Fas	FKCsA	[9]
FKBP	FRB	Rapamycin	[7]
GyrB	GyrB	Coumermycin	[10]
GAI	GID1	Gibberellin	[11]

1-3. Controlling cellular signaling processes with light

Recently, several trials to replace FKBP and FRB with naturally occurring photoreceptors and their binding partners have been reported[12]. The natural photoreceptors and their binding partners form dimers upon irradiation with light. Thus, they act as light-dependent molecular switches alternative to the CID system. In comparison to chemical dimerizers, light generally offers a higher temporal and spatial resolution. In addition, light does not interact with endogenous cellular proteins. Therefore, the approach to control cellular signaling processes with light offers certain advantages over existing CID systems, such as lack of cytotoxicity, rapid activation, reversibility, repeatability and spatial and temporal confinement. The new technology using the combination of genetic and optical methods to control cellular signaling processes with light is called optogenetics[13].

1-4. Naturally occurring photoreceptors

Several optogenetic tools based on naturally occurring photoreceptors and their binding partners have been developed to directly control cellular signaling processes, such as gene expression and cell morphological changes, with light in living cells and organisms[12] (Figure 1-4).

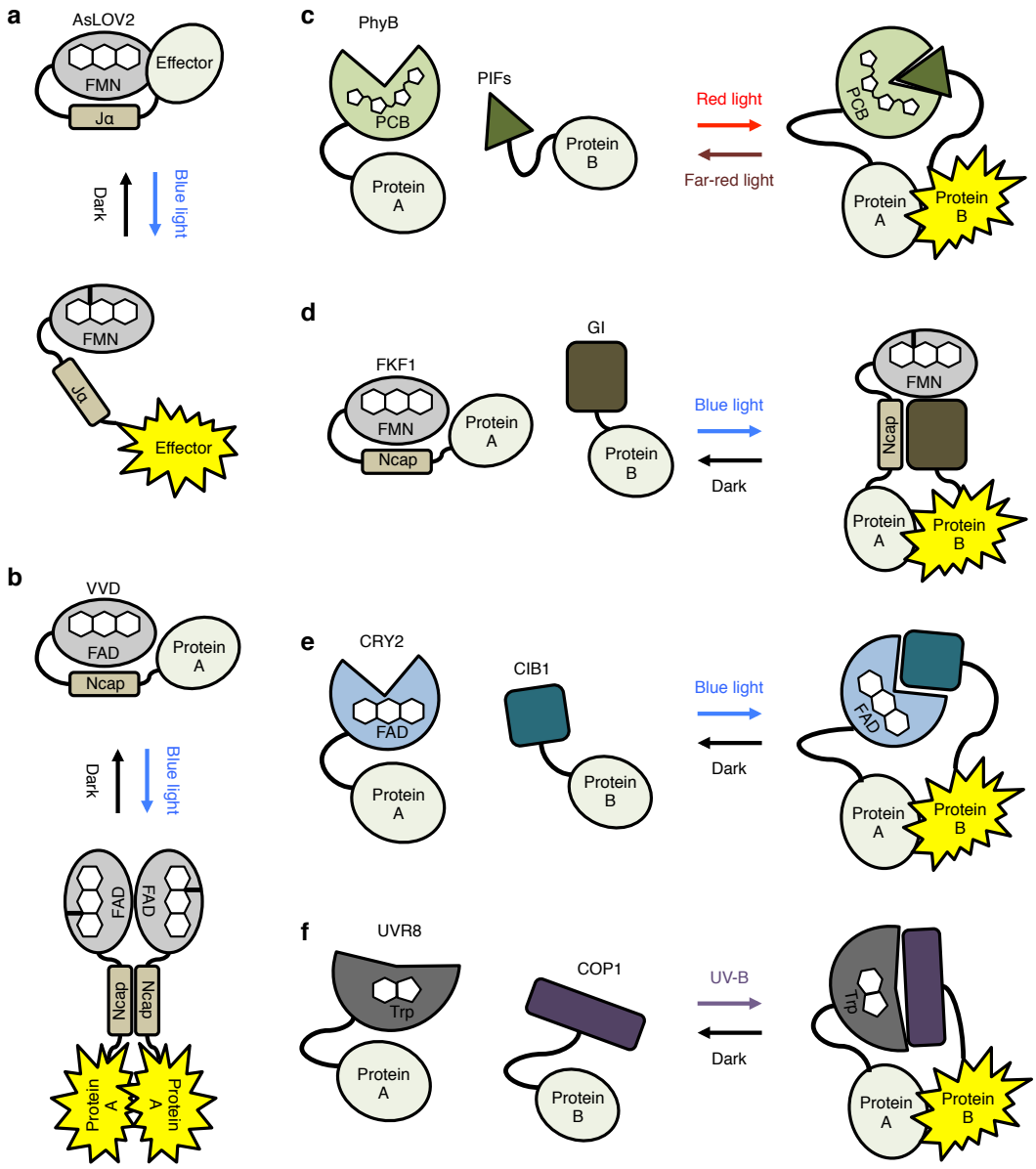

Figure 1-4. Naturally occurring photoreceptors used as photoswitching proteins in existing optogenetic tools. Upon irradiation with light, (**a**) AsLOV2, (**b**) VVD, (**c**) PhyB-PIFs, (**d**) FKF1-GI, (**e**) CRY2-CIB1 and (**f**) UVR8-COP1 form conformational relaxing (a), homodimer (b) and heterodimer (c-f), respectively.

Light-oxygen-voltage (LOV) proteins/domains are popular blue light-absorbing photoreceptors found in plants, fungi and prokaryotes[14]. Representable LOV domains are the second LOV domain of *Avena sativa* phototropin 1 (AsLOV2)[15-18], flavin-binding, Kelch repeat, F-box protein (FKF1)[19] derived from *Arabidopsis thaliana* and *Neurospora crassa* photoreceptor Vivid (VVD)[20]. All share a structurally conserved a Per-Arnt-Sim (PAS) core and helical regions that pack with variable helical elements possibly involved in signal transduction. Upon irradiation with blue light, the LOV domains form a specific covalent bond between a cysteine residue within the PAS core and its binding cofactor (flavin mononucleotide, FMN or flavin-adenine dinucleotide, FAD). This triggers conformational changes in the LOV domains to induce downstream effector functions. For instance, AsLOV2 relaxes the C-terminal α- helix (Jα) to undock from the PAS core upon irradiation with blue light. In other LOV domains, the conformational changes led to dimerization. Eventually, the cysterinly-flavin adduct thermally breaks to return its dark state.

Cryptochromes (CRY1 and CRY2) belong to another class of blue light-absorbing photoreceptors found in plants and animals. To detect blue light, cryptochromes utilize a flavin cofactor FAD as their chromophore. In the case of CRY2, blue light irradiation leads to its dimerization with a differential signaling component, a basic helix-loop-helix protein CIB1[21,22].

Phytochromes are red/far-red light-absorbing photoreceptors found in plants, fungi and bacteria. Phytochromes are commonly composed of PAS, GAF and PHY domains. Phytochrome B (PhyB) is one of the most structurally and biophysically

well characterized red/far-red light absorbing photoreceptors. PhyB and its binding partners, phytochrome interacting factor proteins (PIFs), associate upon irradiation with red light and dissociate upon irradiation with far-red light[23,24].

More recently, several groups have reported a plant photoreceptor derived from *Arabidopsis thaliana* for ultraviolet-B (UV-B), named UV-B resistance locus 8 (UVR8). UVR8 spontaneously forms a homodimer in the dark, but the UVR8 homodimer dissociates upon irradiation with UV-B light, thereby UVR8 interacts with another binding protein, constitutively photomorphogenic 1 (COP1)[25-27].

1-5. Drawbacks of naturally occurring photoreceptors in optogenetics

Existing optogenetic tools based on naturally occurring photoreceptors have opened new avenues in experimental biology, however, naturally occurring photoreceptors often suffer from their unwanted properties (**Table 1-2**). For instance, PhyB-PIFs (PhyB, 908 residues and PIF3, 211 residues and PIF6, 100 residues)[23,24], FKF1-GI (FKF1, 619 residues and GI, 1,173 residues)[19], CRY2-CIB1 (CRY2, 612 residues and CIB1, 355 residues)[21] and UVR8-COP1 (UVR8, 440 residues and COP1, 675 residues)[25,26] are much larger than reporter tags used in fluorescence imaging technologies, such as green fluorescent protein (GFP) derived from the jellyfish Aequorea (238 residues). The large component may increase steric interference in its fusion proteins. PhyB requires a phycobilin cofactor not available in mammalian cells, making its use in mammalian cells difficult because the cofactor must be added exogenously[23,24]. In mammalian cells, FKF1, CRY2 and VVD require no exogenous

cofactor because they bind a flavin cofactor that is abundant in all eukaryotic cells. Also, switch-off kinetics of the naturally occurring photoreceptors are slow (tens of minutes or several hours), thereby preventing them from accurately controlling spatiotemporal activities of cellular proteins[16,19-21,26]. Thus, the naturally occurring photoreceptors have the above serious limitations. Because the nature of photoreceptors used as photoswithcing proteins determines success on failure of optogenetic tools, it is essential for the emerging field of optogenetics to develop robust and versatile photoswitching proteins that overcome these limitations.

Table 1-2. Drowbacks of naturally occurring photoreceptors in optogenetics.

Photoreceptor and binding partner	Molecular size	Cofactor	Swithch-on light	Switch-off light	Switch-off kinetics ($T_{1/2}$)	Lit-state mode	Reference
PhyB / PIF3	908 residues (PIF3, 211 residues)	PφB, PCB	Red	Far-red	–	Heterodimer	[23]
AsLOV2	125 residues	FMN	Blue	–	80 s	conformatioal relaxing	[16-18]
PhyB / PIF6	908 residues (PIF6, 100 residues)	PφB, PCB	Red	Far-red	–	Heterodimer	[24]
FKF1 / GI	619 residues (GI, 1,173 residues)	FMN	Blue	–	1.5 h	Heterodimer	[19]
CRY2 / CIB1	612 residues (CIB1, 355 residues)	FAD	Blue	–	10 min	Heterodimer	[21]
VVD	150 residues	FAD	Blue	–	5 h	Homodimer	[20]
CRY2	612 residues	FAD	Blue	–	10 min	Oligomer	[22]
UVR8	440 residues (COP1, 675 residues)	–	UV-B	–	50 h	Heterodimer	[25–27]

1-6. Purpose of the present study

Chapter 2, I conduct re-engineering of a natural fungal photoreceptor to develop robust and versatile photoswitching proteins. On the basis of a genetic approach, I first engineer the dimer interface of the fungal photoreceptor to prevent the unwanted homo-dimerization and to selectively induce the hetero-dimerization upon irradiation with blue light. Next, to improve the switch-off kinetics of the fungal photoreceptor, I perform additional engineering of the cofactor-binding domain. I also demonstrate that the present photoswitching proteins actually allow spatially and temporally precise control over several signaling proteins in single living cells. This work highlights that re-engineering and improvement of naturally occurring photoreceptors offers new opportunities for the next quantum leap of optogenetic methods to control a wide variety of cellular proteins like marionettes and the related cellular functions at will.

In Chapter 3, I focus on switch-off kinetics of blue light photoreceptors, and develop a high-throughput screening system to efficiently improve its properties. I develop the high-throughput screening system on the basis of fluorescence imaging of thermal reversion of a flavin cofactor bound to blue light photoreceptors. I apply this screening system to AsLOV2, where is one of the most frequently used photoreceptors for optogenetics, and isolate its variants having substantially faster and slower switch-off kinetics, respectively. The present approach is applicable to a variety of blue light-inducible molecular switches and thereby provides a new opportunity for the development of molecular tools for emerging optogenetics.

1-8. Reference

1. Hanahan, D. & Weinberg, R. A. The hallmarks of cancer. *Cell* **100**, 57-70 (2000).
2. Chudakov, D.M., Matz, M.V., Lukyanov, S. & Lukyanov, K.A. Fluorescent proteins and their applications in imaging living cells and tissues. *Physiological reviews* **90**, 1103-1163 (2010).
3. Spencer, D.M., Wandless, T.J., Schreiber, S.L. & Crabtree, G.R. Controlling signal transduction with synthetic ligands. *Science (New York, N.Y.)* **262**, 1019-1024 (1993).
4. Fegan, A., White, B., Carlson, J.C. & Wagner, C.R. Chemically controlled protein assembly: techniques and applications. *Chemical reviews* **110**, 3315-3336 (2010).
5. Putyrski, M. & Schultz, C. Protein translocation as a tool: The current rapamycin story. *FEBS letters* **586**, 2097-2105 (2012).
6. DeRose, R., Miyamoto, T. & Inoue, T. Manipulating signaling at will: chemically-inducible dimerization (CID) techniques resolve problems in cell biology. *Pflug Arch Eur J Phy* **465**, 409-417 (2013).
7. Rivera, V.M., *et al*. A humanized system for pharmacologic control of gene expression. *Nat Med* **2**, 1028-1032 (1996).
8. Ho, S.N., Biggar, S.R., Spencer, D.M., Schreiber, S.L. & Crabtree, G.R. Dimeric ligands define a role for transcriptional activation domains in reinitiation. *Nature* **382**, 822-826 (1996).
9. Belshaw, P.J., Ho, S.N., Crabtree, G.R. & Schreiber, S.L. Controlling protein

association and subcellular localization with a synthetic ligand that induces heterodimerization of proteins. *Proceedings of the National Academy of Sciences of the United States of America* **93**, 4604-4607 (1996).

10. Farrar, M.A., AlberolaIla, J. & Perlmutter, R.M. Activation of the Raf-1 kinase cascade by coumermycin-induced dimerization. *Nature* **383**, 178-181 (1996).
11. Miyamoto, T., *et al*. Rapid and orthogonal logic gating with a gibberellin-induced dimerization system. *Nature chemical biology* **8**, 465-470 (2012).
12. Muller, K. & Weber, W. Optogenetic tools for mammalian systems. *Molecular bioSystems* **9**, 596-608 (2013).
13. Method of the Year 2010. *Nature methods* **8**, 1-1 (2011).
14. Crosson, S., Rajagopal, S. & Moffat, K. The LOV domain family: photoresponsive signaling modules coupled to diverse output domains. *Biochemistry* **42**, 2-10 (2003).
15. Strickland, D., Moffat, K. & Sosnick, T.R. Light-activated DNA binding in a designed allosteric protein. *Proceedings of the National Academy of Sciences of the United States of America* **105**, 10709-10714 (2008).
16. Wu, Y.I., *et al*. A genetically encoded photoactivatable Rac controls the motility of living cells. *Nature* **461**, 104-108 (2009).
17. Pham, E., Mills, E. & Truong, K. A synthetic photoactivated protein to generate local or global Ca(2+) signals. *Chemistry & biology* **18**, 880-890 (2011).
18. Strickland, D., *et al*. TULIPs: tunable, light-controlled interacting protein tags for cell biology. *Nature methods* **9**, 379-384 (2012).

19. Yazawa, M., Sadaghiani, A.M., Hsueh, B. & Dolmetsch, R.E. Induction of protein-protein interactions in live cells using light. *Nature biotechnology* **27**, 941-945 (2009).

20. Wang, X., Chen, X. & Yang, Y. Spatiotemporal control of gene expression by a light-switchable transgene system. *Nature methods* **9**, 266-269 (2012).

21. Kennedy, M.J., *et al*. Rapid blue-light-mediated induction of protein interactions in living cells. *Nature methods* **7**, 973-975 (2010).

22. Bugaj, L.J., Choksi, A.T., Mesuda, C.K., Kane, R.S. & Schaffer, D.V. Optogenetic protein clustering and signaling activation in mammalian cells. *Nature methods* **10**, 249-252 (2013).

23. Shimizu-Sato, S., Huq, E., Tepperman, J.M. & Quail, P.H. A light-switchable gene promoter system. *Nature biotechnology* **20**, 1041-1044 (2002).

24. Levskaya, A., Weiner, O.D., Lim, W.A. & Voigt, C.A. Spatiotemporal control of cell signalling using a light-switchable protein interaction. *Nature* **461**, 997-1001 (2009).

25. Chen, D., Gibson, E.S. & Kennedy, M.J. A light-triggered protein secretion system. *Journal of Cell Biology* **201**, 631-640 (2013).

26. Crefcoeur, R.P., Yin, R.H., Ulm, R. & Halazonetis, T.D. Ultraviolet-B-mediated induction of protein-protein interactions in mammalian cells. *Nat Commun* **4** (2013).

27. Muller, K., *et al*. Multi-chromatic control of mammalian gene expression and signaling. *Nucleic acids research* **41** (2013).

Chapter 2

Engineering pairs of two distinct photoswitching proteins for optogenetic control of cellular proteins

2-1. Introduction

Since the discovery that a macrolide immunosuppressant, known as rapamycin, induces complex formation of two proteins, FKBP12 and mTOR, to provoke cellular responses, FKBP12 and the FKBP12-rapamycin binding (FRB) domain from mTOR have extensively been used as chemically inducible dimerization tags to control activities of cellular proteins, represented by receptors, GTPases, protein kinases and transcription factors[1-4]. These recombinant proteins tagged with FKBP12 and FRB, so-called chemically activatable actuators, have proved that methods for controlling protein activities and thereby perturbing cellular signaling processes provide a powerful approach to a deeper understanding of living cells[5,6]. Recently, several trials to replace FKBP and FRB, which are built in the chemically activatable actuators, with photosensory proteins that form light-inducible dimers, such as photoreceptors and a fluorescent protein, have been reported[7-12]. This is because light is much superior to chemicals in terms of spatial and temporal confinement[13,14]. In particular, several photoreceptors derived from plants and their binding partners, such as phytochrome B (PhyB)-PIFs, cryptochrome 2 (CRY2)-CIB1, and FKF1-GIGANTEA (GI), are being tested as photoswitching proteins to construct photoactivatable actuators[7-10]. However, the naturally occurring photoswitching proteins often suffer from their unwanted properties, such as large molecular sizes, non-mammalian cofactors, low efficiencies and slow kinetics. Because the nature of photoswitching proteins is directly linked to the overall performance of photoactivatable actuators, the development of robust and versatile photoswitching proteins that overcome these limitations is essential for the emerging field of

optogenetics to control cellular proteins with light. Here I conduct re-engineering of a fungal photoreceptor Vivid (VVD) to develop the present pairs of two distinct photoswitching proteins.

2-2. Experimental Section

2-2-1. Plasmids construction and mutagenesis.

I used an N-terminally truncated version (residues 37–186, 17.1 kDa) of VVD because it is more stable than full length VVD (residues 1–186, 21.3 kDa)[15]. cDNA encoding the N-terminally truncated VVD with codons optimized for mammalian expression was synthesized by Invitrogen (Carlsbad, CA, USA). cDNAs encoding the N-terminal frangment (Nfluc: residues 1–398) and C-terminal fragment (Cfluc: residues 394–550) of a firefly luciferase[16] were amplified by a standard PCR approach. Chimeric fusion constructs of VVD and the split-fluc fragments were generated using conventional restriction and ligation methods. cDNAs encoding Nfluc-VVD, VVD-Nfluc, Cfluc-VVD and VVD-Cfluc were subcloned into a mammalian expression vector pcDNA3.1 V5/His-A (Invitrogen) at *Hin*dIII and *Xho*I sites or *Hin*dIII and *Xba*I sites The present mutagenesis of VVD were performed with an overlap extension technique[17] and Multi Site-Directed Mutagenesis Kit (MBL, Nagoya, Aichi, Japan) according to the manufacture's instructions.

cDNAs encoding human Akt1, mouse Tiam1 and human intersectin were obtained from Addgene (Cambridge, MA, USA). cDNAs encoding an inter SH2 domain from bovine p85alpha-PI3kinase (iSH2: residues 421–623)[18], human Akt1 lacking a pleckstrin homology (PH) domain (dAkt1: residues 131–480)[3], a guanine nucleotide exchanging factor (GEF) domain from mouse Tiam1 (Tiam1: residues 1033–1406)[19] and a GEF domain from human intersectin (ITSN: residues 1229–1580)[19] were amplified by a conventional PCR approach. pMagFast1 (VVD-52R/55R/85V) was respectively connected with iSH2, dAkt1, Tiam1 and ITSN

via a flexible polypeptide linker consisting of GGSGGSGGSG using standard PCR, restriction and ligation methods. The cDNAs encoding iSH2-pMagFast1 (PI3K activator unit), dAkt1-pMagFast1 (Akt1 activator unit) and Tiam1-pMagFast1 (Rac1 activator unit) were separately subcloned into the mammalian expression vector pcDNA3.1 V5/His-A at *Hin*dIII and *Xba*I sites. The cDNA encoding ITSN-pMagFast1 (Cdc42 activator unit) was subcloned into a mammalian expression vector with a truncated SV40 promotor to achieve its low expression.

To construct the anchor unit, cDNA encoding humanized monomeric Kikume Green-Red (mKikGR)[20] was obtained from MBL, and amplified by a conventional PCR approach. mKikGR was tagged with a CAAX box motif (QGCMGLPCVVM) derived from C-terminus of N-Ras[21,22] via a flexible polypeptide linker consisting of GGSGG using a standard PCR approach. A chimeric fusion construct of nMagHigh1 (VVD-52D/55G/135I/165I) and mKikGR-CAAX were generated using conventional restriction and ligation methods. A flexible polypeptide linker consisting of GGSGGSGG was inserted between nMagHigh1 and mKikGR-CAAX. The cDNAs encoding nMagHigh1-mKikGR-CAAX (PM anchor unit) was subcloned at *Hin*dIII and *Xho*I sites of the mammalian expression vector, pcDNA3.1 V5/His-A.

The gene encoding TagRFP was obtained from Evrogen (Moscow, Russia), and amplified by a standard PCR approach. Its photostable variant TagRFP-S158T (TagRFP-T)[23] was generated by site-directed mutagenesis. To construct the PI(3,4,5)P_3 biosensor, a PH domain (residues 261-386) derived from human GRP1 (ref. 21) was connected with TagRFP-T via a flexible polypeptide linker consisting of

GGSGGGGSGGGGSGG using standard PCR, restriction and ligation methods. cDNA encoding the PI(3,4,5)P_3 biosensor (PH-TagRFP-T) was subcloned at *Hin*dIII and *Xho*I sites of the mammalian expression vector, pcDNA3.1 V5/His-A.

All cloning enzymes were obtained from Takara Biomedical (Tokyo, Japan) and used according to the manufacturer's instructions. All PCR fragments were sequenced with an ABI310 genetic analyzer (Applied Biosystems, Foster City, CA, USA).

2-2-2. Cell culture.

COS-7 and NIH3T3 cells were cultured at 37 °C under 5% CO_2 in Dulbecco's Modified Eagle Medium (DMEM, Invitrogen, Carlsbad) supplemented with 10% FBS (GIBCO, Carlsbad, CA, USA), 100 unit/ml penicillin and 100 μg/ml of streptomycin (GIBCO). PK15 cells was cultured at 37 °C under 5% CO_2 in Minimum Essential Medium (MEM, Invitrogen) supplemented with 10% FBS, 100 unit/ml penicillin and 100 μg/ml of streptomycin.

2-2-3. Bioluminescence assay.

For the screening of the present VVD variants, COS-7 cells were plated at approximately 2.0×10^4 cells/well in 96-well black-walled plate (Thermo Fisher Scientific, Walthman, MA, USA), and cultured for 24 h at 37 °C in 5% CO_2. The cells were then transfected with a Lipofectamine 2000 reagent (Invitrogen) according to the manufacturer's protocols. cDNAs respectively encoding Nfluc-X and X(Y)-Cfluc (X and Y stand for VVD variants) were transfected at a 1:1 ratio. The

total amount of DNA was 0.4 μg/well. Twenty-four hours after the transfection, the culture medium was replaced with 100 μl of a luciferase assay reagent (Promega, Madison, WI, USA) containing D-luciferin as a substrate. The luciferase assay reagent was prepared by adding 5 ml of Hanks' Balanced Salt Solution (HBSS, Grand Island Biological Co., Grand Island, NY, USA) to one vial of the lyophilized luciferase assay substrate (Promega). After the treatment of the cells with the luciferase assay reagent for 1 h at room temperature, bioluminescence measurements were performed using a Centro XS^3 LB 960 plate-reading luminometer (Berthold Technologies, Bad Wildbad, Germany). Bioluminescence signals were integrated over 10 sec at room temperature. Blue light irradiation was performed using a LED light source (470 nm ± 20 nm) (CCS Inc., Kyoto, Japan). Irradiation time and the intensity of blue light were 30 sec and 3 mW/cm^2, respectively.

For the analysis of the dissociation kinetics of the present VVD variants, COS-7 cells were plated at approximately 10×10^4 cells/well in a 24 well plate (Nunc, Roskilde, Denmark), and cultured for 24 h at 37 °C in 5% CO_2. The cells were then transfected with a Lipofectamine 2000 reagent. cDNAs respectively encoding Nfluc-X and X(Y)-Cfluc were transfected at a 1:1 ratio. The total amount of DNA was 0.8 μg/well. Twenty-four hours after the transfection, the culture medium was replaced with 500 μl of the luciferase assay reagent. The cells were scraped and collected in Röhren polystyrene tubes (Sarstedt, Nümbrecht, Germany). After the treatment of the cells with the luciferase assay reagent for 1 h at room temperature, the sample tube was placed into a Lumat LB 9507 single-tube luminometer (Berthold Technologies), and bioluminescence measurements were performed using the

luminometer. The bioluminescence signals were integrated over 1 sec at room temperature, and plotted every 1 sec. To expose the cells to blue light, I stopped the measurement of bioluminescence intensity, and took out the sample tube from the luminometer. I then irradiated the sample tube with blue light by using the LED light source (470 ± 20 nm, 3 mW/cm^2, 30 sec), and immediately placed back the sample tube into the luminometer to resume the bioluminescence measurement. The time elapsing from the shutoff of blue light irradiation to the resuming of the bioluminescence measurement was less than 1 sec. I fitted the dissociation curves to mono-exponential functions to determine the half lifetime.

2-2-4. Live cell imaging.

Glass-bottomed dishes (Iwaki Glass, Chiba, Japan) were coated with 25 μg/ml of human fibronectin (BD Biosciences, Franklin Lakes, NJ, USA) at room temperature for 1 h, and then washed twice with 2 ml of Milli-Q water. To conduct the PI(3,4,5)P_3 imaging, PK15 cells were plated at approximately 2.0 × 10^4 cells/dish on the glass-bottomed dishes, and cultured for 24 h at 37 °C in 5% CO_2. The cells were co-transfected with cDNAs encoding the PI3K activator unit, the PM anchor unit and the PI(3,4,5)P_3 biosensor in a 1:6:1 ratio by using the Lipofectamine 2000 reagent. The total amount of DNA was 0.8 μg/dish. Twelve hours after the transfection, the medium was replaced by a MEM culture medium supplemented with 10% FBS. The cells were maintained for 24~30 h at 28 °C. Before fluorescence imaging, the cells were incubated with HBSS containing 25 mM HEPES supplemented by 2% bovine serum albumin (BSA, Wako, Osaka, Japan) for at least 3 h. Live cell

imaging was conducted at 28 °C with a 63× oil objective (Carl Zeiss, Jena, Germany) on the stage of a LSM 710 confocal laser scanning microscope (Carl Zeiss) with a heated stage adaptor (Tokai Hit Co., Fujinomiya, Shizuoka, Japan). Fluorescence images of mKikGR and TagRFP-T were taken using a Multi-line Argon laser (514 nm) and a HeNe laser (543 nm), respectively. Blue light irradiation of whole cells was conducted using a Multi-line Argon laser (488 nm) with a power density of 2 mW.

To control cell morphology using the Magnet-based photoactivatable actuators, NIH3T3 cells were plated at approximately 0.8×10^4 cells/dish on glass-bottomed dishes coated with fibronectin, and cultured for 24 h at 37 °C in 5% CO_2. The cells were co-transfected with the PI3K activator and PM anchor units in a 1:3 ratio by using the Lipofectamine 2000 reagent. Similarly, the Akt1, Rac1 and Cdc42 activator units were separately co-transfected, along with the PM anchor unit. The total amount of DNA was 0.8 μg/dish. Twenty-four hours after the transfection, the cells were incubated with DMEM containing 25 mM glucose, 25 mM HEPES and no phenol red (Grand Island Biological Co.) supplemented with 2% BSA for at least 3 h before cell morphology controlling. Live cell imaging was conducted at 37 °C with a 63× oil objective on the stage of a LSM 710 confocal laser scanning microscope with a heated stage adaptor. DIC images of the cells were taken every 30 sec using a HeNe laser (633 nm) with minimal laser power and scan time at 2.55 μsec/pixel. Blue light irradiation of an edge part of the cells was repeatedly conducted using a Multi-line Argon laser (488 nm) with a power density of 0.25 mW. Pharmacological inhibition of PI3K and that of Akt1 were performed with LY294002

(Sigma Chemical Co., St Louis, MO, USA) and AKT inhibitor IV (Calbiochem, San Diego, CA, USA), respectively.

2-3. Results

2-3-1. Design of a pair of two distinct VVD variants that discriminate each other based on electrostatic interactions.

VVD is a photoreceptor that regulates a blue light response of a filamentous fungus, *Neurospora crassa*[24] (**Figure 2-1a**). VVD has competitive advantages as follows: It is one of the smallest photoreceptors among those tested for photoactivatable actuators so far. Its cofactor is flavin adenine dinucleotide (FAD) that is abundant in any biological systems. In addition, the photoreceptor reversibly switches its state from a monomer to a homo-dimer in response to blue light[15,24,25]. Such a dynamic dimerization property of VVD confers a potential advantage as a versatile photoswitching protein on the photoreceptor. However, its homo-dimerization property causes serious technological problems, as chemically inducible homo-dimerization proteins[5,26] earlier than FKBP12-FRB have also suffered. This is because when VVD is used as a photoswitching protein to bring two different proteins (protein A and protein B) close to each other, the photoreceptor induces not only an A-B pair but also unwanted A-A and B-B pairs with light (**Figure 2-1b**). This prevents efficient induction of the intended A-B pair and causes serious side effects resulting from the A-A and B-B pairs. In the present study, to suppress the formation of the unwanted A-A and B-B pairs and to selectively induce the intended A-B pair with light, I first engineer the dimer interface of VVD.

An N-terminal α-helix, termed Ncap (Ile47 to Asn56), is located in the dimer interface of VVD[24,25] and consisted of neutral amino acids. I develop two distinct types of VVD variants: One with substitutions with positively charged amino

acids in the Ncap and the other with negatively charged amino acids there (**Figure 2-1a, c**). Different from VVD, the two types of VVD variants discriminate each other based on electrostatic interactions (attraction and repulsion): The electrostatic attraction is advantageous to the blue light-dependent hetero-dimerization of the VVD variants, while the electrostatic repulsion prevents their homo-dimerization (**Figure 2-1c**). This is how the two types of VVD variants rule out the possibility that the unwanted A-A and B-B pairs are induced, thereby selectively triggering the induction of the expected A-B pair with light (**Figure 2-1c**).

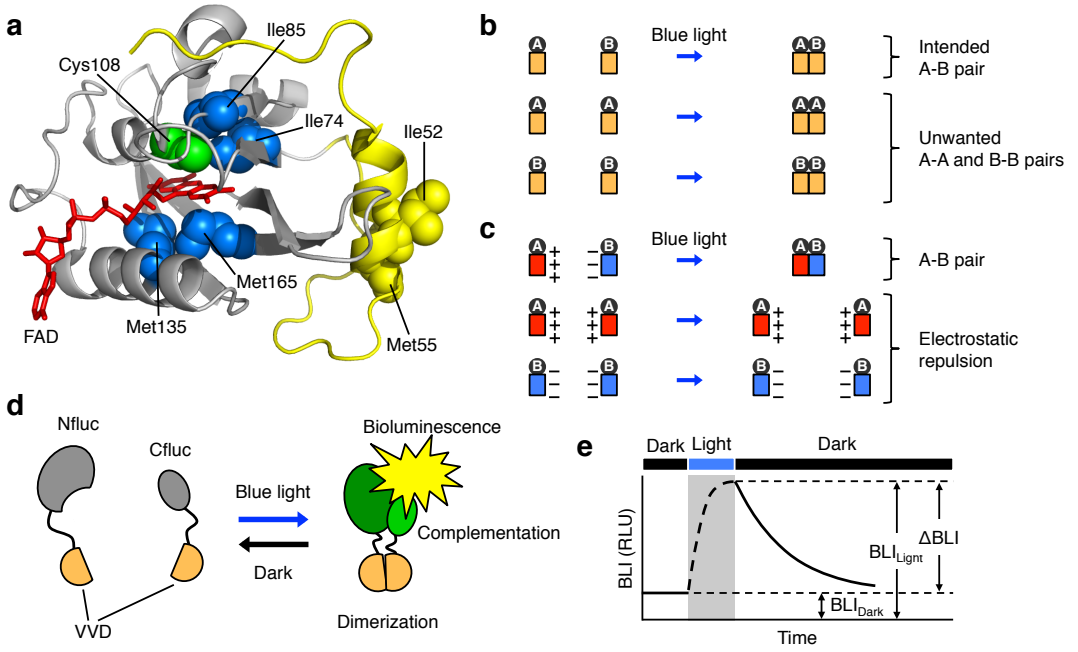

Figure 2-1. Engineering the dimer interface of VVD. (**a**) Structure of VVD and its key amino acid residues for the present study. Blue light irradiation triggers the formation of a photo-adduct between Cys108 (green) and the isoalloxazine ring of FAD (red), thereby inducing dimerization of VVD. The Ncap (yellow) is located in the interface of the dimer. Photocycle-related residues are shown in blue. (**b**) When used as a photoswitching protein, VVD (orange square) induces not only the pairing of protein A and protein B but also the unwanted A-A and B-B pairs in response to blue light. (**c**) The present two distinct types of VVD variants (red and blue squares) prevent the homo-dimerization and selectively induce the hetero-dimerization based on electrostatic interactions. (**d**) A schematic of the bioluminescence assay system that reports dimerization of VVD. One VVD is tagged with an N-half fragment (Nfluc) of a split-firefly luciferase and the other with its C-half fragment (Cfluc). These separate fusions are monomers under the dark condition, thereby having no bioluminescence activity. Upon blue light irradiation, quick dimerization of VVD leads to rapid complementation of Nfluc and Cfluc, inducing bioluminescence signals. This assay system allows reversible detection of the VVD dimerization and its dissociation. (**e**) A schematic diagram of the measurement and the evaluation of the VVD dimerization. Bioluminescence intensities (BLIs) under the dark condition and after blue light irradiation are represented by BLI_{Dark} and BLI_{Light}, respectively. ΔBLI is calculated by subtracting BLI_{Dark} from BLI_{Light}. RLU, relative light unit.

2-3-2. Engineering the dimer interface of VVD.

I developed a bioluminescence assay system based on complementation of split-firefly luciferase fragments[16] to monitor the blue light-dependent dimerization of VVD and its variants (**Figure 2-1d, e** and **Figures 2-2**). Using this system, I search out key amino acid residues in the Ncap of VVD, of which substitutions lead to the expected electrostatic discrimination. I separately substituted each of amino acid residues from 47 to 56 in the Ncap with a glutamic acid, and picked up variants, of which homo-dimerization was impaired due to electrostatic repulsion by the negatively charged amino acid. The single substitutions of the amino acid residues, except for Asn56, resulted in a substantial decrease in homo-dimerization of the VVD variants upon blue light irradiation (**Figure 2-3a**). In particular, the single substitution of Ile47, Met48, Tyr50, Leu51, Ile52, Ile54 or Met55 with a glutamic acid was more effective to lower the ratio of the bioluminescence intensity (BLI) under the light condition (BLI_{Light}) to that under the dark condition (BLI_{Dark}). These BLI ratios (BLI_{Light}/BLI_{Dark}) were comparable to that of the nonfunctional variant VVD-C71S[24] (**Figure 2-3a**). I separately substituted each of the amino acid residues 47, 48, 50, 51, 52, 54 and 55 of VVD with an arginine. Then, each of the arginine (R)-variants was mixed with each of the glutamic acid (E)-variants, both of which have single substitutions at the amino acid residue 47, 48, 50, 51, 52, 54 or 55, and examined hetero-dimerization of the variants (**Figure 2-3b**). Among the VVD variants, the pair of the 52R-variant and the 52E-variant and that of the 55R-variant and the 55E-variant gave substantially increased BLIs upon blue light irradiation (**Figure 2-3b**). Also, the single substitution of Ile52 or Met55 was more effective to

differentiate the BLI_{Light}/BLI_{Dark} ratios between the hetero-dimerization and the homo-dimerization than others (**Figure 2-3c**).

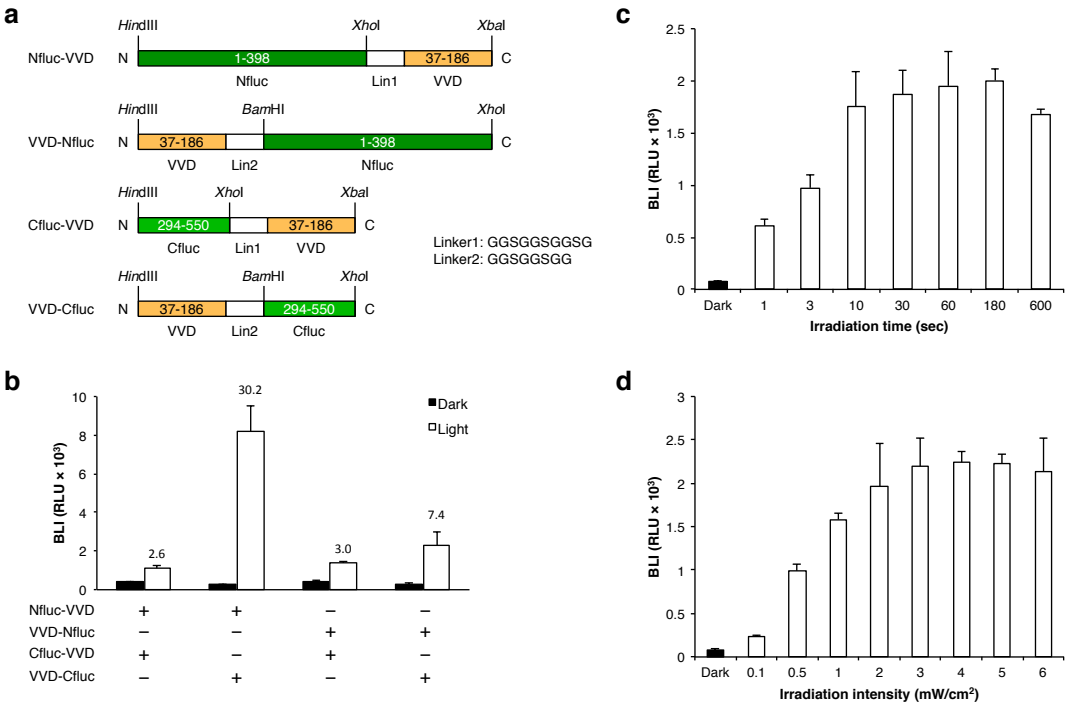

Figure 2-2. A bioluminescence assay system for monitoring dimerization of VVD based on complementation of split-firefly luciferase fragments. (**a**) Schematic representations of domain structures of the fusion proteins tested in Figure 2-2b. An N-half fragment (Nfluc) and a C-half fragment (Cfluc) of a split-firefly luciferase were separately tagged with VVD with different orientations. (**b**) Detecting blue light-dependent dimerization of VVD with split luciferase fragments. COS-7 cells co-expressing Nfluc-VVD or VVD-Nfluc along with Cfluc-VVD or VVD-Cfluc were irradiated with blue light (470 ± 20 nm, 3 mW/cm^2) for 30 s. The pair of Nfluc-VVD and VVD-Cfluc produced a larger bioluminescence signal than others in response to blue light. BLI, bioluminescence intensity; RLU, relative light unit. The ratio of BLI_{Light} to BLI_{Dark} is shown above each bar. The result is means ± S.D. of three independent measurements. (**c**, **d**) Optimizing conditions for the irradiation to induce the VVD dimerization. (c) COS-7 cells co-expressing Nfluc-VVD and VVD-Cfluc were irradiated with blue light (470 ± 20 nm, 3 mW/cm^2) for 1, 3, 10, 30, 60, 180 and 600 s, respectively. The bioluminescence intensity reached the maximum level upon blue light irradiation with a power density at 3 mW/cm^2 for 30 s. (d) COS-7 cells co-expressing Nfluc-VVD and VVD-Cfluc were irradiated for 30 s with 0.1, 0.5, 1, 2, 3, 4, 5 and 6 mW/cm^2 blue light, respectively. The bioluminescence intensity reached the maximum level upon blue light irradiation with a power density at 3 mW/cm^2 for 30 s. The results are means ± S.D. of three independent measurements.

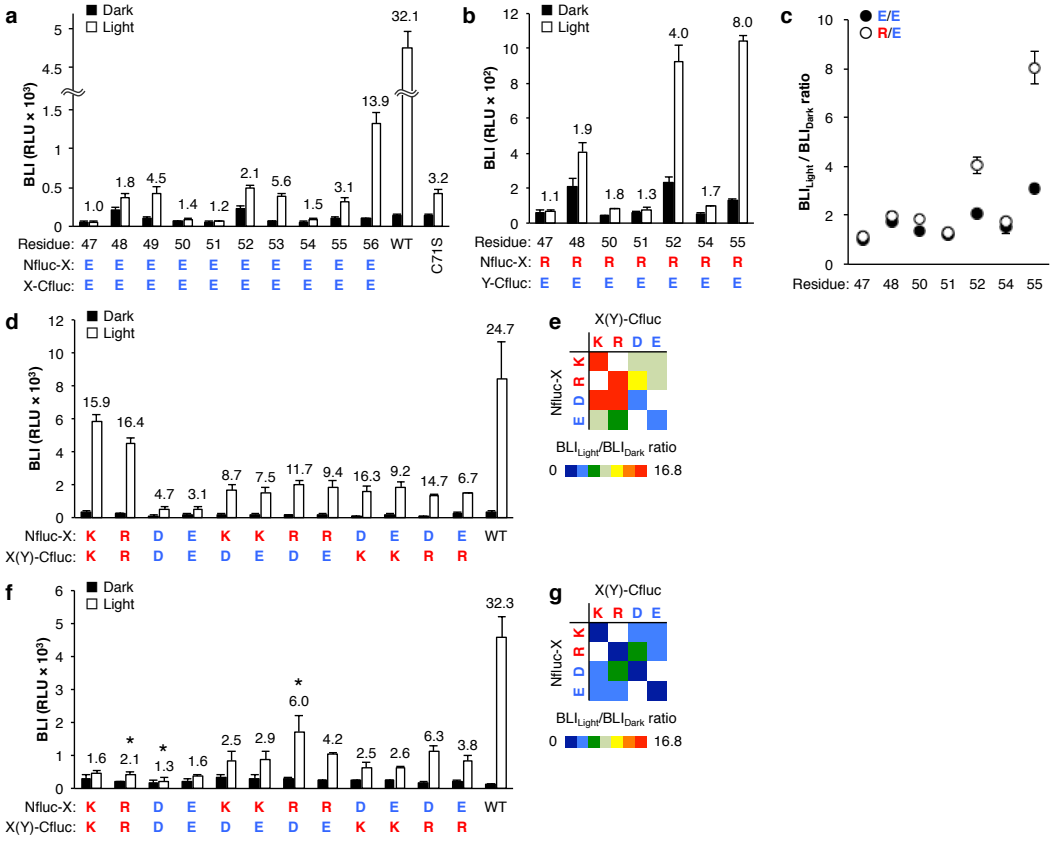

Figure 2-3. Electrostatic interactions-based discrimination of the hetero-dimer from the homo-dimer. (**a**) Homo-dimerization of VVD variants, having single substitutions with a glutamic acid at amino acid residues from 47 to 56, respectively. Nfluc-X and X(Y)-Cfluc (X and Y stand for VVD variants) were co-expressed in COS-7 cells. The cells were irradiated with blue light (470 ± 20 nm, 3 mW/cm^2) for 30 s, and bioluminescence measurements of the live cells were then performed. The BLI_{Light}/BLI_{Dark} ratio is shown above each white bar. (**b**) Hetero-dimerization of each of the arginine (R)-variants and each of the glutamic acid (E)-variants, both having single substitutions at amino acid residue 47, 48, 50, 51, 52, 54 or 55. (**c**) A comparison of the BLI_{Light}/BLI_{Dark} ratio between the homo-dimerization (closed circle) and the hetero-dimerization (open circle) of the VVD variants having single substitutions of amino acid residue 47, 48, 50, 51, 52, 54 or 55. (**d**, **f**) Homo-dimerization and hetero-dimerization of VVD variants having single substitution with a charged amino acid at amino acid residue 55 (d) or 52 (f). (**e**, **g**) Heat maps of the BLI_{Light}/BLI_{Dark} ratios shown in Figure 2-3d,f, respectively. The results are means ± S.D. of three independent measurements. Single asterisks highlight VVD-52R and VVD-52D.

To comprehensively examine the effect of single substitution of Ile52 or Met55 with a charged amino acid on both of the homo-dimerization and the hetero-dimerization, I also constructed aspartic acid (D)-variants and lysine (K)-variants in addition to the E-variants and R-variants. In the case of Met55, its single substitution with a negatively charged amino acid suppressed homo-dimerization of the VVD variants, and hetero-dimerization was promoted between the variants with a negatively charged amino acid and those with a positively charged amino acid (**Figure 2-3d,e**). However, single substitution of Met55 with a positively charged amino acid did not inhibit homo-dimerization of the VVD variants (**Figure 2-3d,e**). This is in contrast to the case of substitution of Ile52. The single substitution of Ile52 suppressed not only homo-dimerization of the VVD variants with a negatively charged amino acid but also that with a positively charged amino acid (**Figure 2-3f,g**). In addition, the single substitution of Ile52 was effective to promote hetero-dimerization of the VVD variants with a negatively charged amino acid and those with a positively charged amino acid (**Figure 2-3f,g**). Among the VVD variants with single substitutions of Ile52, the pair of the R-variant (VVD-52R) and the D-variant (VVD-52D) was more effective to promote the hetero-dimerization than others.

As shown above, the amino acid residue 52 plays a key role as a primary site for the development of the present photoswitching proteins based on electrostatic interactions. However, it has not escaped our notice that the amino acid residue 55 can also be an important site for the purpose because its single substitution with a charged amino acid was effective to promote the hetero-dimerization of the VVD

variants (**Figure 2-3d**). I thus conducted mutagenesis of Met55 of both VVD-52R and VVD-52D. Substitution of Met55 of VVD-52R and that of VVD-52D with a charged amino acid were effective to more suppress the homo-dimerization of VVD-52R and that of VVD-52D (**Figure 2-4a**). However, the double substitutions of both the residues 52 and 55 with a charged amino acid were not effective for the hetero-dimerization (**Figure 2-4b,d**).

In the process of investigation of the VVD variants with the double substitutions, I found that VVD-52R/55R with arginine substitutions of both the residues 52 and 55 efficiently formed a hetero-dimer with VVD-52D having no substitution of Met55 (**Figure 2-4c,d**). This implies that as the residue 55 of VVD variants having the 52D substitution, uncharged amino acids may be more promising compared with charged amino acids to achieve efficient hetero-dimerization with VVD-52R/55R. Thus I substituted Met55 of VVD-52D with other fifteen uncharged amino acids, respectively, and examined the hetero-dimerization with VVD-52R/55R and the homo-dimerization (**Figure 2-4e,f**). I found that among the VVD variants, the glycine-variant (VVD-52D/55G) was more effective to promote hetero-dimerization with VVD-52R/55R (**Figure 2-4e**). This pair also exhibited a largely improved BLI_{Light}/BLI_{Dark} ratio (**Figure 2-4e**), compared with the pair of VVD-52R and VVD-52D (**Figure 2-3f**). In addition, VVD-52D/55G was more effective to prevent the homo-dimerization than others (**Figure 2-4f**). As a result of double substitutions of both the residues 52 and 55 of VVD, the pair of VVD-52R/55R and VVD-52D/55G was obtained as the most promising pair of two distinct VVD variants that discriminate each other based on electrostatic interactions.

Hereafter, the present VVD variants are collectively referred to as “Magnet” after a pair of metallic magnets that discriminate each other through both of the attraction and the repulsion. In particular, VVD-52R/55R and VVD-52D/55G, having positively charged arginine at the residue 52 and negatively charged aspartic acid there, are named “positive Magnet (pMag)” and “negative Magnet (nMag)”, respectively.

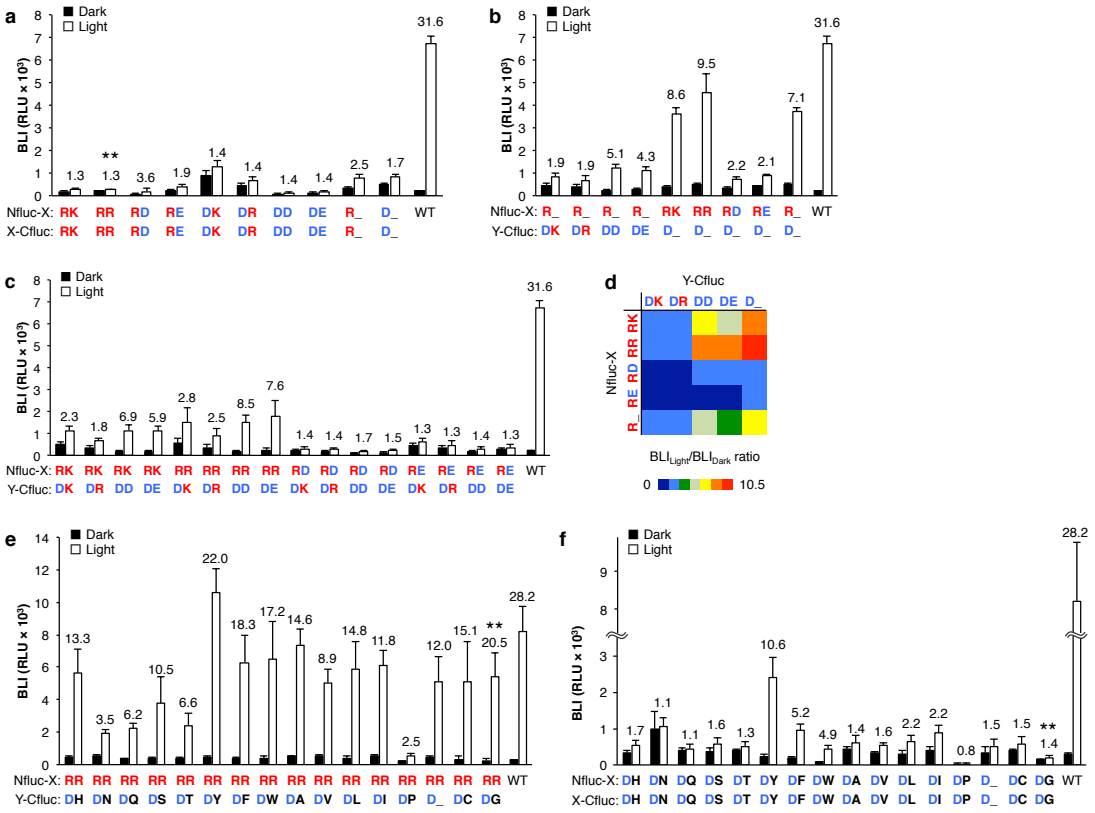

Figure 2-4. Electrostatic interactions-based discrimination of the hetero-dimer from the homo-dimer. (**a**) Homo-dimerization of VVD variants having double substitutions with a charged amino acid at amino acid residues 52 and 55. Two-letter code with R, K, D and E represents each of VVD variants with arginine, lysine, aspartic acid and glutamic acid at amino acid residues 52 and 55 (e.g., RK stands for VVD-52R/55K). VVD-52R and VVD-52D, having no substitution at amino acid residue 55, are depicted as R_ and D_, respectively. (**b**) Hetero-dimerization of VVD variants having double substitutions with a charged amino acid at amino acid residues 52 and 55. (**c**) Hetero-dimerization between VVD-52R or VVD-52D and each of VVD variants having substitution with a charged amino acid at amino acid residue 55 of VVD-52D or VVD-52R. (**d**) A heat map of the BLI_{Light}/BLI_{Dark} ratios shown in Figure 2-4b,c. (**e**) Hetero-dimerization between VVD-52R/55R and each of VVD variants having substitution with an uncharged amino acid at amino acid residue 55 of VVD-52D. (**f**) Homo-dimerization of VVD variants with double substitutions with an uncharged amino acid at amino acid residues 52 and 55. The results are means ± S.D. of three independent measurements. Double asterisks highlight VVD-52R/55R and VVD-52D/52G, renamed pMag and nMag, respectively.

2-3-3. Engineering photoswitching proteins with enhanced kinetics and dimerization efficiencies.

Next I address the kinetic aspect of Magnet. pMag and nMag form a hetero-dimer quickly upon blue light irradiation (**Figure 2-5a**). However, it takes hours before the complex dissociates when the blue light is shut off ($T_{1/2}$ = 2.2 h) (**Figure 2-5a**). The slow dissociation kinetics of the pMag-nMag complex is similar to that of the homo-dimer of VVD ($T_{1/2}$ = 2.5 h) (**Figure 2-6a**). If the dissociation of the pMag-nMag complex becomes much faster than it is through additional mutagenesis, such variants must provide a powerful tool for spatially and temporally more confined optical control of cellular proteins. Previous studies on flavin-binding domains of various photoreceptors have suggested that amino acid residues surrounding the isoalloxazine ring of the flavin cofactor govern photocycle, that is, a reaction cycle of blue light-dependent flavin-cysteinyl adduct formation and its subsequent break in the dark condition[27-30]. In the case of VVD, several amino acid residues were identified as key residues that control the kinetics of the photocycle[28]. In particular, substitutions of Ile74 and/or Ile85 and that of Met135 and/or Met165 within the flavin-binding domain of VVD were reported to significantly shorten and lengthen the photocycle, respectively (**Figure 2-5a**). I introduced the photocycle-related substitutions into both pMag and nMag, and examined dissociation kinetics of the complex of the variants.

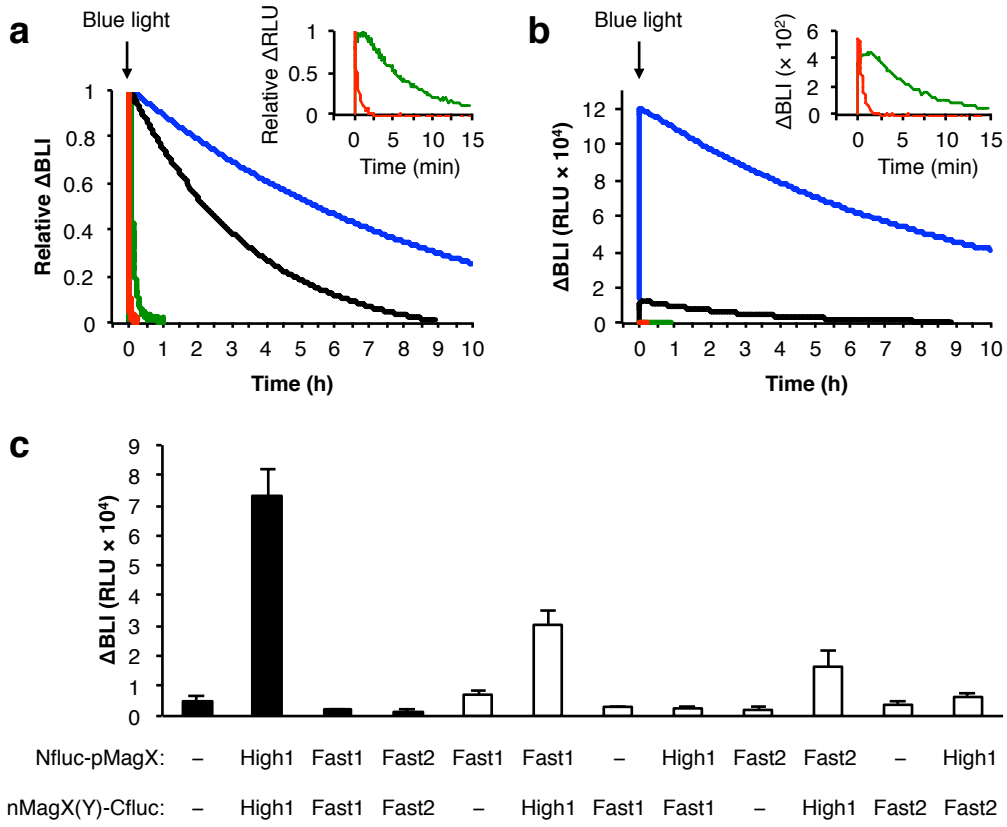

Figure 2-5. Magnet pairs with substantially enhanced dimerization efficiencies and accelerated dissociation kinetics. (**a**) Dissociation kinetics of the complexes of pMag-85V and nMag-85V (green, also shown in the inset), pMag-74V/85V and nMag-74V/85V (red, also shown in the inset), pMag and nMag (black), and pMag-135I/165I and nMag-135I/165I (blue). COS-7 cells co-expressing Nfluc-pMagX and nMagX-Cfluc (X stands for 85V, 74V/85V or 135I/165I variant) were irradiated with blue light at time 0 for 30 s to induce the complex formation, and the observation of its dissociation was followed. (**b**) Changing the photocycles of Magnets substantially affects the extent of their dimerization upon blue light irradiation. The data shown in Figure 2-5b is essentially the same as that in Figure 2-5a, except that the ΔBLIs in Figure 2-5a is normalized, while the other is not normalized. (**c**) nMagHigh1 substantially enhances the extent of dimerization. pMagX and nMagX(Y) stand for Magnet variants. Fast1, Fast2, n-dash (–) and High1 stand for p(n)MagFast1, p(n)MagFast2, p(n)Mag and p(n)MagHigh1, respectively. As well as pMag and nMag, homo-dimerization of these variants is suppressed due to the electrostatic repulsion (Figure 2-6b). The result is means ± S.D. of three independent measurements. Arrows show the time points of repeated blue light irradiations. The results (a) and (b) represent typical experiments from three independent measurements.

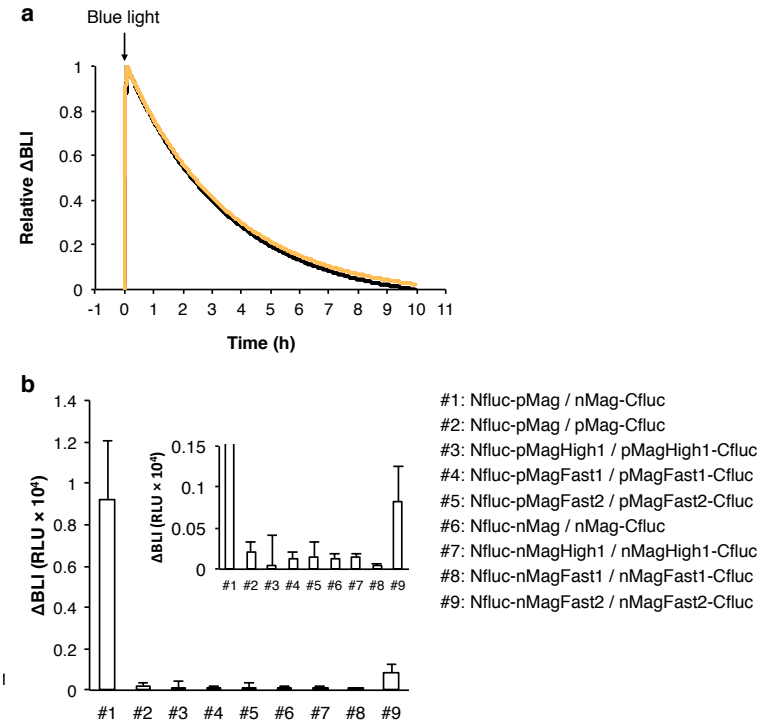

Figure 2-6. (**a**) Dissociation kinetics of the pMag-nMag hetero-dimer (black) and the VVD-VVD homo-dimer (orange). COS-7 cells expressing the pair of Nfluc-pMag and nMag-Cfluc or that of Nfluc-VVD and VVD-Cfluc were irradiated with blue light (470 ± 20 nm, 3 mW/cm^2) for 30 s. The homo-dimer of VVD dissociated with a half lifetime of 2.5 h, similar to the pMag-nMag hetero-dimer ($T_{1/2}$ = 2.2 h). The result represents typical experiments from three independent measurements. (**b**) Homo-dimerization of pMag variants and that of nMag variants. COS-7 cells co-expressing the Nfluc-X and X-Cfluc (X stands for any one of Magnet variants shown in the figure) were irradiated with blue light (470 ± 20 nm, 3 mW/cm^2) for 30 s. The pMag variants and the nMag variants do not efficiently form their homo-dimers upon blue light irradiation. ΔBLI was obtained by subtracting BLI_{Dark} from BLI_{Light}. The result is means ± S.D. of three independent measurements.

When Ile85 of both pMag and nMag were substituted with a valine, the complex of pMag-85V and nMag-85V dissociated with a half lifetime of 5.3 min, 25-fold faster than the pMag-nMag complex (**Figure 2-5a**). The complex of pMag-74V/85V and nMag-74V/85V, having substitutions of both Ile74 and Ile85 with a valine, exhibited substantially accelerated dissociation ($T_{1/2}$ = 24 s), 330-fold faster than the pMag-nMag complex (**Figure 2-5a**). The result shows that substitutions, which shorten the photocycle in the case of VVD, make the dissociation of the complex of the pMag and nMag variants fast. I renamed pMag-85V "pMagFast1" and nMag-85V "nMagFast1", respectively. Likewise, pMag-74V/85V and nMag-74V/85V were renamed "pMagFast2" and "nMagFast2", respectively. I also showed that substitutions of both Met135 and Met165 with an isoleucine, which lengthen the photocycle in the case of VVD, slow the dissociation of the complex of pMag-135I/165I and nMag-135I/165I ($T_{1/2}$ = 5.4 h) (**Figure 2-5a**).

The bioluminescence assay not only reports the dissociation kinetics of the complexes of the pMag and nMag variants but also provides quantitative information about the extent of their dimerization upon blue light irradiation. I found that bioluminescence signals upon dimerization of pMag-135I/165I and nMag-135I/165I, having long photocycles and slow dissociation kinetics, increased up to 1500% of that of pMag and nMag (**Figure 2-5b,c**). This shows that the 135I/165I substitutions introduced into pMag and nMag substantially enhance the extent of their blue light-dependent dimerization. I renamed pMag-135I/165I "pMagHigh1" and nMag-135I/165I "nMagHigh1", respectively. In contrast to these two, I found that bioluminescence signals upon dimerization of pMagFast1 and nMagFast1 and that of

pMagFast2 and nMagFast2, having short photocycles and fast dissociation kinetics, decreased to 45% and 36% of that of pMag and nMag, respectively (**Figure 2-5b,c**). The result shows that changing the photocycles of pMag and nMag substantially affects the extent of dimerization of the variants, and particularly reveals a negative functional correlation between fast dissociation kinetics and dimerization efficiency. However, such an unwanted trade-off is unacceptable to develop useful photoswitching proteins. To overcome this limitation, I examine blue light-dependent hetero-dimerization between a pMag variant and an nMag variant, having each different dissociation kinetics (**Figure 2-5c**).

I found that the extent of hetero-dimerization of pMagFast1 and nMagHigh1, having fast and slow dissociation kinetics, respectively, was enhanced up to 1,400% of dimerization of pMagFast1 and nMagFast1 (**Figure 2-5c**). In the case of hetero-dimerization of pMagFast2 and nMagHigh1, such enhancement was observed up to 960% of the extent of dimerization of pMagFast2 and nMagFast2 (**Figure 2-5c**). The result indicates that pairing with nMagHigh1 substantially enhances the inefficient dimerization extent of the pMag variants having fast dissociation kinetics. What is even better is that nMagHigh1 does not slow the dissociation kinetics of its hetero-dimers with the fast pMag variants (**Figure 2-7a,b**). The pMagFast1-nMagHigh1 complex dissociated with a half lifetime of 11 min, similar to the pMagFast1-nMagFast1 complex ($T_{1/2}$ = 5.3 min) (**Figure 2-5a**). Another pMagFast2-nMagHigh1 complex dissociated with a half lifetime of 44 s, comparable to the pMagFast2-nMagFast2 complex ($T_{1/2}$ = 24 s) (**Figure 2-5b**). In particular, the dissociation kinetics of pMagFast2-nMagHigh1 is strikingly faster than

conventional blue-light photoswitching proteins based on naturally occurring photoreceptors. For example, CRY2-CIB1 requires several tens of minutes to dissociation after shutting blue light off[10]. The other photoswitching protein, FKF1-GI, does not dissociate in 1.5 hours at least[9]. In addition, the pairing of nMagHigh1 and the pMag variants did not prevent the reversible dimerization properties of the pMag variants (**Figure 2-7c,d**). The present approach based on hetero-dimerization between the variants having each different dissociation kinetics has thus solved the unwanted trade-off problem and allowed us to develop the present pairs of two distinct photoswitching proteins with both substantially enhanced dimerization efficiencies and accelerated dissociation kinetics (**Table 2-1**).

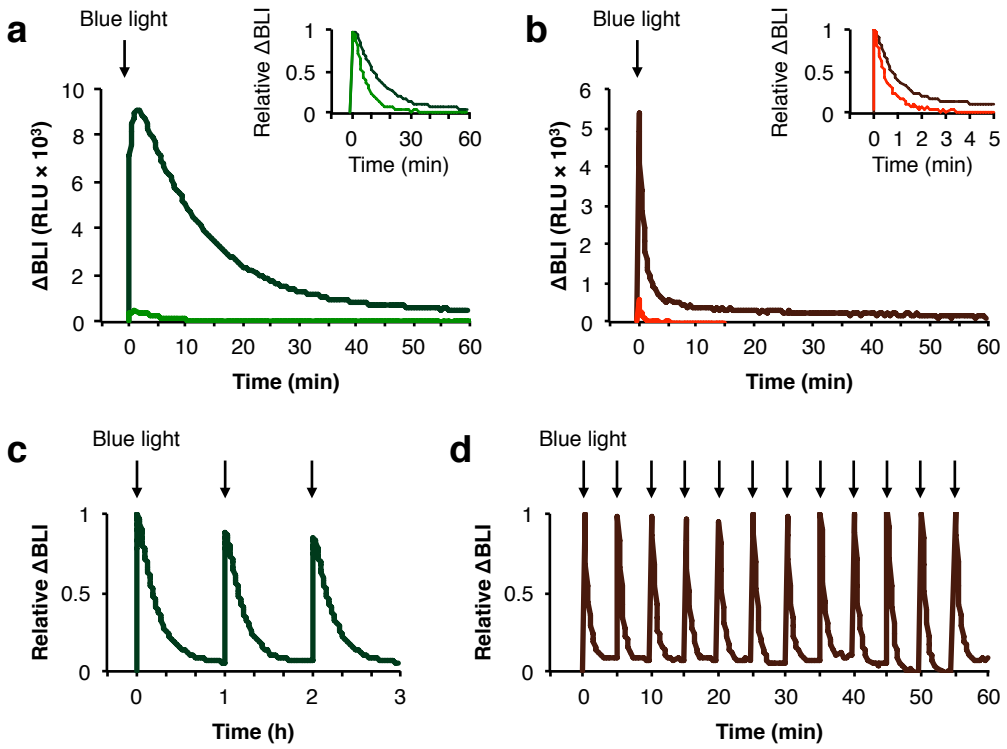

Figure 2-7. Magnet pairs with substantially enhanced dimerization efficiencies and accelerated dissociation kinetics. (**a**) Dissociation kinetics of the pMagFast1-nMagFast1 (green) and pMagFast1-nMagHigh1 (dark green) complexes. The inset shows relative ΔBLIs. (**b**) Dissociation kinetics of pMagFast2-nMagFast2 (red) and pMagFast2-nMagHigh1 (dark red). (**c**, **d**) Reversible dimerization and dissociation properties of pMagFast1-nMagHigh1 (c) and pMagFast2-nMagHigh1 (d). Arrows show the time points of repeated blue light irradiations. The results (a) though (d) represent typical experiments from three independent measurements.

Table 2-1. Properties of pairs of Magnet variants

Pairs of Magnet variants	Substitutions	Dimerization efficiency	Half lifetime of dissociation kinetics (s)
pMag	52R/55R	100%	7,920
nMag	52D/55G		
pMagFast1	52R/55R/85V	45%	318
nMagFast1	52D/55G/85V		
pMagFast2	52R/55R/74V/85V	36%	24
nMagFast2	52D/55G/74V/85V		
pMagHigh1	52R/55R/135I/165I	1,500%	19,400
nMagHigh1	52D/55G/135I/165I		
pMagFast1	52R/55R/85V	1,400%	660
nMagHigh1	52D/55G/135I/165I		
pMagFast2	52R/55R/74V/85V	960%	44
nMagHigh1	52D/55G/135I/165I		

2-3-4. Spatially and temporally precise optical control of cellular proteins with Magnet.

Next I show that the present photoswitching proteins enable optical control of cellular proteins and the related cellular functions. As an example, I connected pMagFast1 with an inter SH2 (iSH2) domain[18] derived from a p85 regulatory subunit of phosphatidylinositol 3-kinase (PI3K) (**Figure 2-8a,b**). When expressed in the cell, the fusion protein of pMagFast1 and the iSH2 domain, termed a PI3K-activator unit, spontaneously binds to an endogenous p110 catalytic subunit of PI3K that is responsible for the production of a lipid messenger, phosphatidylinositol 3,4,5-triphosphate ($PI(3,4,5)P_3$). Another photoswitching protein, nMagHigh1, is tethered to the plasma membrane (PM) by connecting with a CAAX box motif[21,22] derived from N-Ras (**Figure 2-8a,b** and **Figure 2-9**). I named it a PM-anchor unit. Upon irradiation of the cell with blue light, the PI3K-activator unit is recruited to the plasma membrane through hetero-dimerization of pMagFast1 and nMagHigh1 (**Figure 2-8a**), thereby inducing the rapid production of $PI(3,4,5)P_3$ in the plasma membrane (**Figure 2-8c**, **2-10** and **2-11**). The Magnet-based PI3K-activator and PM-anchor units thus function as photoactivatable actuators to generate $PI(3,4,5)P_3$, that is, photoactivatable PI3K.

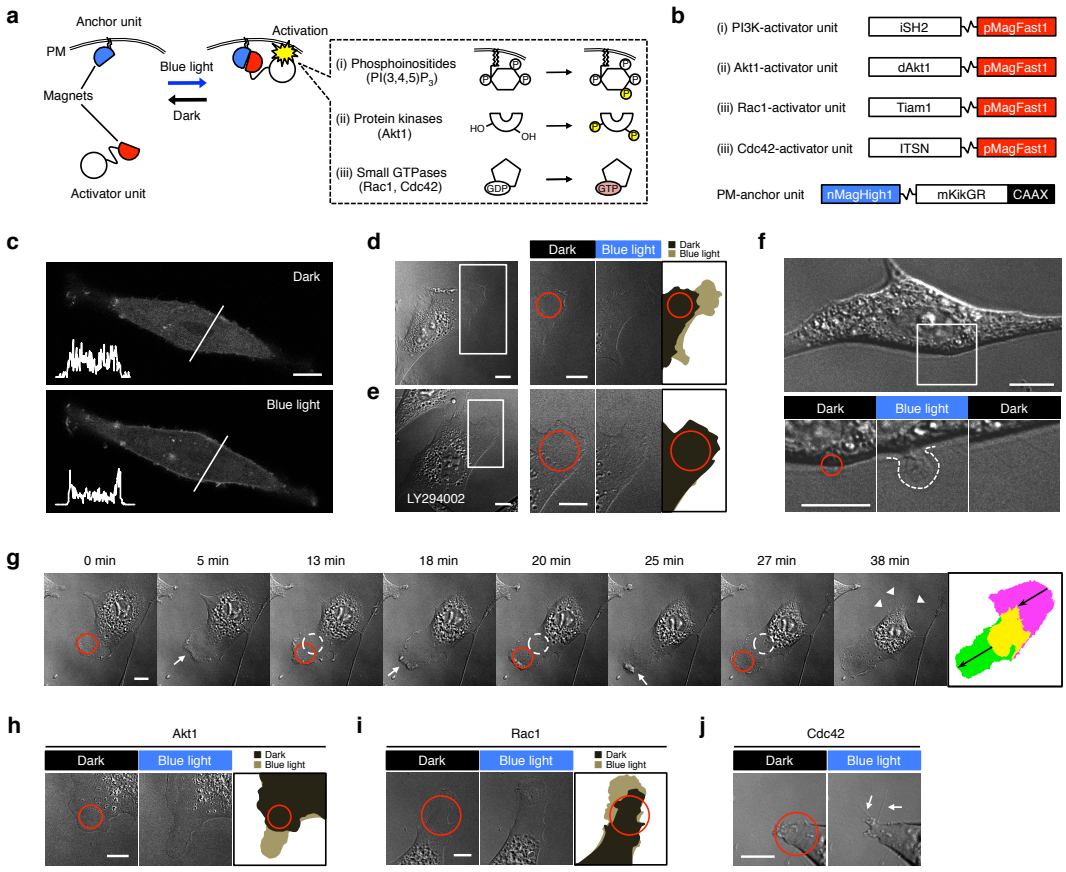

Figure 2-8. Magnet-based photoactivatable actuators. (**a**) A schematic diagram of Magnet-based photoactivatable actuators (activator and PM-anchor units). The activator unit is recruited to the PM-anchor unit tethered to the plasma membrane (PM) upon blue light irradiation. (**b**) Schematic representations of domain structures of the activator and PM-anchor units. (**c**) Fluorescence images of a cell expressing a fluorescent PI(3,4,5)P_3-biosensor consisting of TagRFP-T and a pleckstrin homology domain from GRP1 that specifically binds to PI(3,4,5)P_3. The cell is also expressed with the PI3K-activator and PM-anchor units (Magnet-based photoactivatable PI3K). Global irradiation of the cell with blue light (488 nm) induced the translocation of the PI(3,4,5)P_3-biosensor from the cytosol to the plasma membrane. Line profiles (white) shown in images represent fluorescence intensities of TagRFP-T before and after blue light irradiation. (**d**) Spatial control of the formation of membrane protrusions after focal irradiation (red) at 488 nm of the cell using Magnet-based photoactivatable PI3K. Schematics of the cell edge before (dark brown) and after (light brown) the blue light irradiation are shown in the right panel. (**e**) Treatment of the cell with a PI3K inhibitor LY294002 (50 μM) blocks the blue light-dependent formation of membrane protrusions. (**f**) More spatially and temporally confined irradiation of a quiescent

cell edge, where no lamellipodia are spontaneously generated. Bottom panels show DIC images before (left) and after (center) focal irradiation at 488 nm in a small part (red, 3.0 μm) of the cell. A small lamellipodium (width 3.7 μm, length 4.8 μm) that is generated after blue light irradiation is highlighted with a dotted and curved white line. In the right panel, a DIC image 6 min after the blue light is turned off is shown. (**g**) Directional cell migration guided by repeated and gradually moving irradiation (red) at 488 nm of the cell expressing Magnet-based photoactivatable PI3K. The firstly irradiated position is represented by a white circle. Schematics of the cell position before blue light irradiation (magenta) and 38 min after the first irradiation (green) are shown in the right panel. Arrows show membrane protrusions and ruffling in the leading edge of the cell. Arrowheads show membrane retraction in the rear side of the cell. (h–j) NIH3T3 cells were separately expressed with the Akt1-activator (**h**), Rac1-activator (**i**) and Cdc42-activator (**j**) units. All of these cells are co-expressed with the PM-anchor unit. The cells were focally irradiated at 488 nm in an edge part (red) of the cell. Schematics of the cell edge before (dark brown) and after (light brown) the blue light irradiation are shown in the right panels, respectively. Arrows show the formation of filopodia. The results (c) through (j) represent typical experiments from three independent measurements. Scale bar, 10 μm.

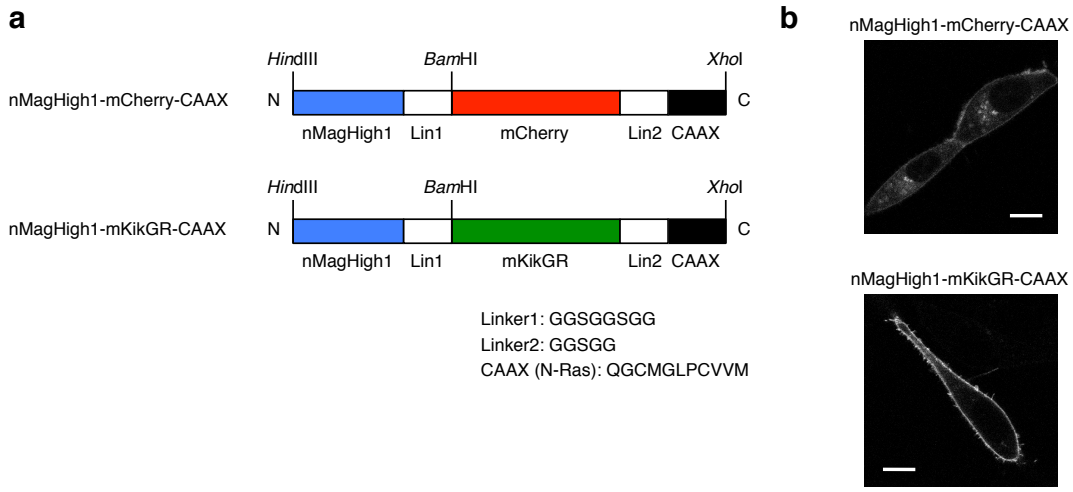

Figure 2-9. A comparison of subcellular localization between the PM-anchor unit tagged with mCherry and that with mKikGR. (**a**) Schematic representations of domain structures of nMagHigh1-mCherry-CAAX and nMagHigh1-mKikGR-CAAX. (**b**) A fluorescence image of NIH3T3 cells expressed with nMagHigh1-mCherry-CAAX (upper panel) and that with nMagHigh1-mKikGR-CAAX (bottom panel). The cells were imaged with a confocal microscope. The mCherry domain caused aggregate formation of the PM-anchor unit and its mislocalizaiotn in the cell, whereas the mKikGR domain allowed proper localization of the PM-anchor unit in the plasma membrane. The result represents typical experiments from three independent measurements. Scale bar, 10 μm.

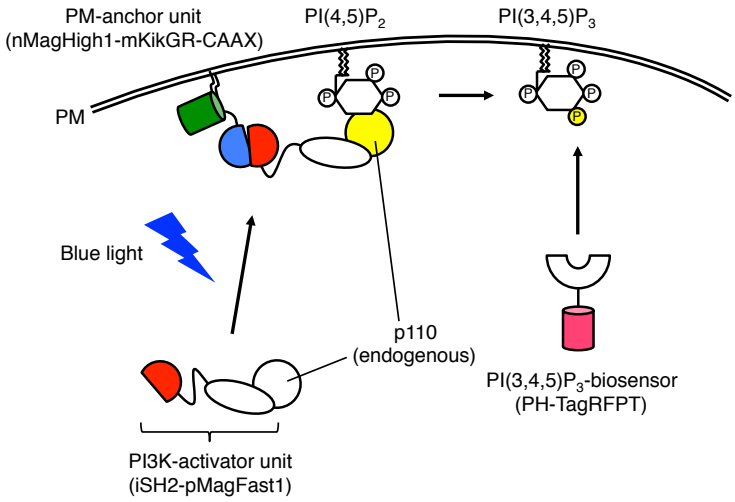

Figure 2-10. A schematic diagram of Magnet-based photoactivatable actuators for PI3K. Blue light irradiation recruits the PI3K-activator unit (iSH2-pMagFast1) constitutively bound with endogenous p110 catalytic subunit of PI3K to the plasma membrane through the interaction with the PM-anchor unit (nMagHigh1-mKikGR-CAAX), and induced the PI3K activation there. Activated PI3K generates $PI(3,4,5)P_3$ by phosphorylating $PI(4,5)P_2$ in the plasma membrane. The $PI(3,4,5)P_3$ production is imaged with the $PI(3,4,5)P_3$-biosensor, a fusion protein of TagRFP-T and a pleckstrin homology domain from GRP1 that specifically binds to $PI(3,4,5)P_3$.

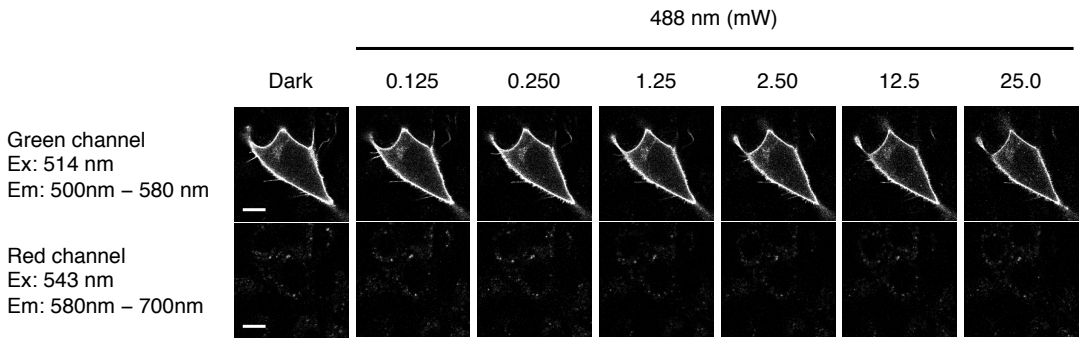

Figure 2-11. Blue light (488 nm) used for the Magnet-based photoactivatable actuators (0.25~2.0 mW) does not induce the photoconversion of mKikGR built in the PM-anchor unit. When NIH3T3 cells expressing the PM-anchor (nMagHigh1-mKikGR-CAAX) unit were sequentially irradiated at 488 nm with a power density of 0.125, 0.250, 1.25, 2.50, 12.5 and 25.0 mW, respectively, no significant green-to-red photoconversion was observed for mKikGR. Each fluorescence image was obtained after irradiation with blue light with the indicated power densities under a confocal microscope. The result represents typical experiments from three independent measurements. Scale bar, 10 μm.

$PI(3,4,5)P_3$ is a lipid messenger that plays a critical role in the regulation of morphological changes in the leading edge of migrating cells[31]. Focal irradiation of the cell that expresses photoactivatable PI3K rapidly induced protrusions, known as lamellipodia, and ruffles in the irradiated part of the plasma membrane (**Figure 2-8d**). These morphological changes were blocked by pretreatment of the cell with LY294002, a potent inhibitor for PI3K (**Figure 2-8e**), confirming that the observed lamellipodia formation and membrane ruffling were direct consequences of the irradiation-dependent production of $PI(3,4,5)P_3$ through photoactivatable PI3K.

I conducted more spatially and temporally confined irradiation of a quiescent part of the plasma membrane, where no lamellipodia spontaneously appeared (**Figure 2-8f**). A small lamellipodium was rapidly generated in the irradiated small part of the plasma membrane. The small lamellipodium shrank and disappeared when the light is turned off. This indicates that photoactivatable PI3K allows rapid and reversible generation of enough amount of $PI(3,4,5)P_3$ to induce lamellipodia formation even in the quiescent part of the plasma membrane at high spatiotemporal patterns. Next I repeatedly performed focal irradiation of the cell with gradually moving the position of irradiation (**Figure 2-8g**). Lamellipodia and ruffles were continuously induced in the irradiated part of the plasma membrane, as seen in naturally occurring leading edges of migrating cells. The cell subsequently moved to the direction guided with light. On the opposite side of the irradiated cell edge, membrane retraction was observed, as seen in naturally occurring rear side of migrating cells. Magnet-based photoactivatable PI3K thus induces cell polarity and allows directional cell movement with light.

In addition to PI3K, I developed Magnet-based photoactivatable actuators for a protein kinase (Akt1)[19] and two small GTPases (Rac1 and Cdc42)[19], which are also involved in the regulation of morphological changes in the plasma membrane of migrating cells. To construct an Akt1-activator unit, I replaced the iSH2 domain of the PI3K-activator unit with an Akt1 variant (dAkt1)[3] that lacks a pleckstrin homology (PH) domain responsible for its translocation to the plasma membrane upon cellular stimulations (**Figure 2-8d**). In response to blue light, Magnet-based photoactivatable Akt1 induced a striking morphological change in the irradiated part of the plasma membrane, leading to local formation of lamellipodia and membrane ruffles (**Figure 2-8h**). The morphological change was blocked by pretreatment of the cell with an inhibitor for Akt1 (**Figure 2-12**). The result indicates that Magnet drive the spatiotemporal activation of Akt1 with light.

In the case of the small GTPases, I connected pMagFast1 with a guanine nucleotide exchanging factor (GEF) domain derived from Tiam1 (ref. 19) and that from intersectin[19] to construct a Rac1-activator unit and a Cdc42-activator unit, respectively (**Figure 2-8b**). Magnet-based photoactivatable Rac1 induced lamellipodia formation in the irradiated part of the plasma membrane (**Figure 2-8i**), while Magnet-based photoactivatable Cdc42 induced a different morphological change from lamellipodia, known as filopodia (**Figure 2-8j**). This is consistent with previous reports[19] showing that Rac1 and Cdc42 are respectively involved in the regulation of the distinct morphological changes in the plasma membrane of migrating cells. The results demonstrate that the present photoswithches provide a robust tool to spatially and temporally control a variety of cellular proteins and the

related cellular functions with light.

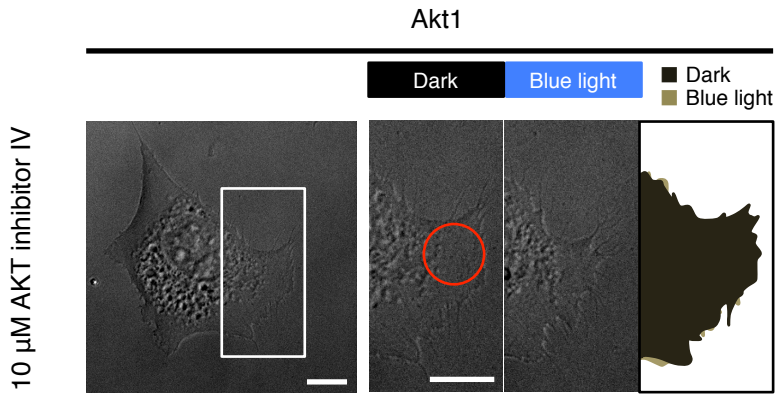

Figure 2-12. AKT inhibitor IV blocks Magnet-based photoactivatable Akt1. NIH3T3 cells expressing the Akt1-activator and PM-anchor units were treated 10 μM AKT inhibitor IV for 1 h, and then an edge part (red) of the cell was focally irradiated at 488 nm. Morphological changes induced by Magnet-based photoactivatable Akt1 were blocked by the pretreatment of the cell with AKT inhibitor IV, confirming that Magnet-based photoactivatable Akt1 actually drives the activation of the protein kinase with light. A schematic representation of a cell edge before blue light irradiation (dark brown) and 30 min after the irradiation (light brown) is also shown in the right panel. The result represents typical experiments from three independent measurements.

2-4. Discussion

I have carried out re-engineering of the fungal photoreceptor VVD and created the present pairs of two distinct photoswitching proteins, named Magnet (**Figure 2-13**). Before completing the development, I have faced three hurdles. First I engineered the dimer interface of VVD both to prevent the unwanted homo-dimerization and to selectively induce the hetero-dimerization upon blue light irradiation. This has generated a pair of two distinct VVD variants that discriminate each other based on electrostatic interactions introduced into the dimer interface. Next, to speed up the dissociation kinetics of the hetero-dimer, additional engineering of the cofactor-binding domain was performed. This has pinpointed a functional link between the dissociation kinetics of the hetero-dimer and its dimerization efficiency, and generated two types of contrasting variants: One with ~330-fold accelerated dissociation kinetics but diminished dimerization efficiencies, and the other with 15-fold enhanced dimerization efficiencies but slower dissociation kinetics. I have solved the trade-off problem by pairing the two contrasting variants and created the present photoswitching proteins with both substantially enhanced dimerization efficiencies and accelerated dissociation kinetics. Magnet thus overcomes limitations of VVD and thereby outperform existing interaction-based photoswhitching proteins.

Different from red/far-red light photoswitching proteins (PhyB-PIFs)[8] that require a plant bilin cofactor not available in mammalian cells, Magnet binds to a flavin cofactor that is abundant in any biological systems as well as conventional blue light photoswitching proteins (CRY2-CIB1 and FKF1-GI)[9,10]. The conventional blue

light photoswitching proteins and Magnet thus require no additional cofactors when used in mammalian cells in contrast to the red/far-red light photoswitching proteins. Furthermore, Magnet (150 amino acids) is much smaller than any other conventional photoswitching proteins, CRY2 (612 a.a.)-CIB1 (355 a.a.), FKF1 (619 a.a.)-GI (1,173 a.a.) and PhyB (908 a.a.)-PIFs (PIF3, 211 a.a. and PIF6, 100 a.a.), because this is derived from the smallest photoreceptor VVD. This is why the present Magnet minimizes the steric hindrance and greatly facilitates accurate molecular design and fine-tuning of photoactivatable actuators. In addition to these advantages, Magnet acquires the kinetic superiority as a result of the present re-engineering. pMagFast2-nMagFast2 ($T_{1/2}$ = 24 sec) and pMagFast2-nMagHigh1 ($T_{1/2}$ = 44 sec), pMagFast1-nMagFast1 ($T_{1/2}$ = 5.3 min) and pMagFast1-nMagHigh1 ($T_{1/2}$ = 11 min) are much faster to dissociate than any other conventional blue light photoswitching proteins, CRY2-CIB1 (ref. 10) (~several tens of minutes) and FKF1-GI[9] (not dissociate in 1.5 hours at least). In particular, pMagFast2-nMagHigh1 and pMagFast1-nMagHigh1 are also devised to exhibit greatly enhanced dimerization efficiencies without sacrificing the fast dissociation kinetics. Magnet thus allows faster and more spatially and temporally precise optical control of cellular proteins than conventional blue light photoswitching proteins. The present study offers not only Magnet with fast dissociation kinetics but also those with slow dissociation kinetics, such as pMag-nMag ($T_{1/2}$ = 2.2 h) and pMagHigh1-nMagHigh1 ($T_{1/2}$ = 5.4 h). Such a tunable property of Magnet may allow various optogenetic applications with each different time range from seconds to hours.

Besides the naturally occurring conventional photoswitching proteins, that is, CRY2-CIB1, FKF1-GI and PhyB-PIFs, Strickland *et al*. have recently reported engineered blue light photoswitching proteins, termed TULIPs, based on an interaction between a PDZ domain and its target peptide[11]. This engineering approach allows tuning of the sensitivity of TULIPs by changing the PDZ-peptide affinity. However, because the PDZ-peptide interaction is naturally occurring in most of mammalian cells, the PDZ domain and its target peptide used for TULIPs can respectively interact with endogenous target proteins and PDZ domain-containing proteins in mammalian cells. This prevents efficient function of TULIPs and causes unwanted side effects, such as mislocalization of TULIPs and subsequent uncontrollable activation or inactivation of molecular processes in the cell. The present Magnet does not suffer from this technological problem because this does not use any interactions naturally occurring in mammalian cells.

Magnet that outperforms existing interaction-based photoswitching proteins provides a robust and versatile tool for powerful optogenetic applications. I have described Magnet-based photoactivatable actuators for PI3K (lipid kinase), Akt1 (protein kinase), Rac1 (small GTPase) and Cdc42 (small GTPase). Potential target proteins to be optically controlled with Magnet is not limited to lipid kinases, protein kinases and small GTPases, but appears to cover a wide variety of cellular proteins, including those which have already been shown to be turned chemically activatable by tagging with FKBP12 and FRB, such as receptors[1], transcription factors[4], phosphatases[18] and heterotrimeric G proteins[32]. In addition, recently emerging methodologies, represented by split protein complementation[33], reported for a

recombinase, proteases, metabolic enzymes, etc., are potentially applicable to the controlled activation of cellular proteins. These related methodologies may also lead to further expansion of the variation of the target proteins that can be turned photoactivatable by tagging with Magnet. Due to their robustness and general applicability, Magnet may also have a significant impact on the related research fields, represented by synthetic biology, where controlled activation of cellular proteins is highly required. The present photoswitching proteins, created by re-engineering of the nature of the naturally occurring photoreceptor, provide new opportunities for the next technological leap of optogenetic methods to control a wide variety of cellular proteins like marionettes and the related cellular functions at will.

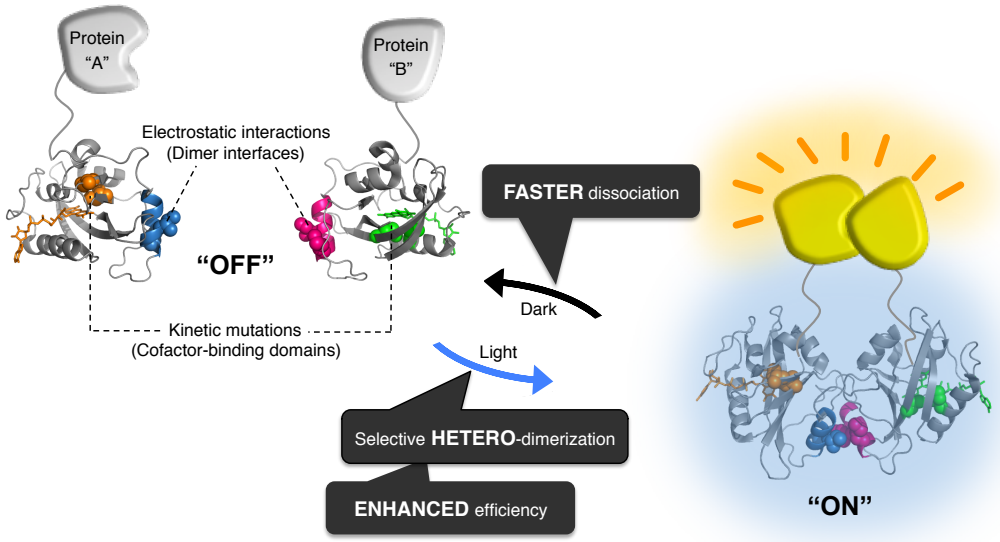

Figure 2-13. Re-engineering of the nature of a fungal photoreceptor has created pairs of two distinct photoswitching proteins with selective hetero-dimerization properties, substantially enhanced dimerization efficiencies and accelerated dissociation kinetics, allowing spatially and temporally precise control of cellular proteins with light.

2-5. References

1. Spencer, D.M., Wandless, T.J., Schreiber, S.L. & Crabtree, G.R. Controlling signal transduction with synthetic ligands. *Science* **262**, 1019-24 (1993).
2. Enomoto, A. et al. Akt/PKB regulates actin organization and cell motility via Girdin/APE. *Dev Cell* **9**, 389-402 (2005).
3. Li, B., Desai, S.A., MacCorkle-Chosnek, R.A., Fan, L. & Spencer, D.M. A novel conditional Akt 'survival switch' reversibly protects cells from apoptosis. *Gene Ther* **9**, 233-44 (2002).
4. Liberles, S.D., Diver, S.T., Austin, D.J. & Schreiber, S.L. Inducible gene expression and protein translocation using nontoxic ligands identified by a mammalian three-hybrid screen. *Proc Natl Acad Sci U S A* **94**, 7825-30 (1997).
5. Fegan, A., White, B., Carlson, J.C. & Wagner, C.R. Chemically controlled protein assembly: techniques and applications. *Chem Rev* **110**, 3315-36 (2010).
6. Putyrski, M. & Schultz, C. Protein translocation as a tool: The current rapamycin story. *FEBS Lett* **586**, 2097-105 (2012).
7. Tyszkiewicz, A.B. & Muir, T.W. Activation of protein splicing with light in yeast. *Nat Methods* **5**, 303-5 (2008).
8. Levskaya, A., Weiner, O.D., Lim, W.A. & Voigt, C.A. Spatiotemporal control of cell signalling using a light-switchable protein interaction. *Nature* **461**, 997-1001 (2009).
9. Yazawa, M., Sadaghiani, A.M., Hsueh, B. & Dolmetsch, R.E. Induction of protein-protein interactions in live cells using light. *Nat Biotechnol* **27**, 941-5 (2009).

10. Kennedy, M.J. et al. Rapid blue-light-mediated induction of protein interactions in living cells. *Nat Methods* **7**, 973-5 (2010).

11. Strickland, D. et al. TULIPs: tunable, light-controlled interacting protein tags for cell biology. *Nat Methods* **9**, 379-84 (2012).

12. Zhou, X.X., Chung, H.K., Lam, A.J. & Lin, M.Z. Optical control of protein activity by fluorescent protein domains. *Science* **338**, 810-4 (2012).

13. Wu, Y.I. et al. A genetically encoded photoactivatable Rac controls the motility of living cells. *Nature* **461**, 104-8 (2009).

14. Baker, M. Direct protein control. *Nature Methods* **9**, 443-447 (2012).

15. Zoltowski, B.D. & Crane, B.R. Light activation of the LOV protein vivid generates a rapidly exchanging dimer. *Biochemistry* **47**, 7012-9 (2008).

16. Paulmurugan, R. & Gambhir, S.S. Combinatorial library screening for developing an improved split-firefly luciferase fragment-assisted complementation system for studying protein-protein interactions. *Anal Chem* **79**, 2346-53 (2007).

17. Ho, S.N., Hunt, H.D., Horton, R.M., Pullen, J.K. & Pease, L.R. Site-directed mutagenesis by overlap extension using the polymerase chain reaction. *Gene* **77**, 51-9 (1989).

18. Suh, B.C., Inoue, T., Meyer, T. & Hille, B. Rapid chemically induced changes of PtdIns(4,5)P2 gate KCNQ ion channels. *Science* **314**, 1454-7 (2006).

19. Inoue, T., Heo, W.D., Grimley, J.S., Wandless, T.J. & Meyer, T. An inducible translocation strategy to rapidly activate and inhibit small GTPase signaling pathways. *Nat Methods* **2**, 415-8 (2005).

20. Habuchi, S., Tsutsui, H., Kochaniak, A.B., Miyawaki, A. & van Oijen, A.M. mKikGR, a monomeric photoswitchable fluorescent protein. *PLoS One* **3**, e3944 (2008).

21. Sato, M., Ueda, Y., Takagi, T. & Umezawa, Y. Production of PtdInsP3 at endomembranes is triggered by receptor endocytosis. *Nat Cell Biol* **5**, 1016-22 (2003).

22. Sato, M., Ueda, Y. & Umezawa, Y. Imaging diacylglycerol dynamics at organelle membranes. *Nat Methods* **3**, 797-9 (2006).

23. Shaner, N.C. et al. Improving the photostability of bright monomeric orange and red fluorescent proteins. *Nat Methods* **5**, 545-51 (2008).

24. Zoltowski, B.D. et al. Conformational switching in the fungal light sensor Vivid. *Science* **316**, 1054-7 (2007).

25. Vaidya, A.T., Chen, C.H., Dunlap, J.C., Loros, J.J. & Crane, B.R. Structure of a light-activated LOV protein dimer that regulates transcription. *Sci Signal* **4**, ra50 (2011).

26. Pollock, R. & Clackson, T. Dimerizer-regulated gene expression. *Curr Opin Biotechnol* **13**, 459-67 (2002).

27. Christie, J.M. et al. Steric interactions stabilize the signaling state of the LOV2 domain of phototropin 1. *Biochemistry* **46**, 9310-9 (2007).

28. Zoltowski, B.D., Vaccaro, B. & Crane, B.R. Mechanism-based tuning of a LOV domain photoreceptor. *Nat Chem Biol* **5**, 827-34 (2009).

29. Zoltowski, B.D., Nash, A.I. & Gardner, K.H. Variations in protein-flavin hydrogen bonding in a light, oxygen, voltage domain produce non-Arrhenius

kinetics of adduct decay. *Biochemistry* **50**, 8771-9 (2011).

30. Conrad, K.S., Bilwes, A.M. & Crane, B.R. Light-Induced Subunit Dissociation by a Light-Oxygen-Voltage Domain Photoreceptor from Rhodobacter sphaeroides. *Biochemistry* **52**, 378-91 (2013).
31. Haugh, J.M., Codazzi, F., Teruel, M. & Meyer, T. Spatial sensing in fibroblasts mediated by 3' phosphoinositides. *J Cell Biol* **151**, 1269-80 (2000).
32. Putyrski, M. & Schultz, C. Switching heterotrimeric G protein subunits with a chemical dimerizer. *Chem Biol* **18**, 1126-33 (2011).
33. Shekhawat, S.S. & Ghosh, I. Split-protein systems: beyond binary protein-protein interactions. *Curr Opin Chem Biol* **15**, 789-97 (2011).

Chapter 3

Fluorescence imaging-based high-throughput screening of fast- and slow-cycling LOV proteins

3-1. Introduction

Blue light photoreceptors and photosensory domains derived from plants and fungi have been tested as light-inducible molecular switches or photoswitching proteins to optogenetically control specific molecular processes in living cells, such as cellular signaling processes and gene expression[1] (**Figure 3-1a**). However, these natural photoswitching proteins suffer from their slow switch-off kinetics[2-6] that prevents them from accurately controlling spatiotemporal activities of cellular proteins[7]. If photoswitching proteins with faster switch-off kinetics than natural photoswitching proteins become available through mutagenesis, they should provide a powerful tool for more spatially and temporally confined optical control of protein activities in the cells.

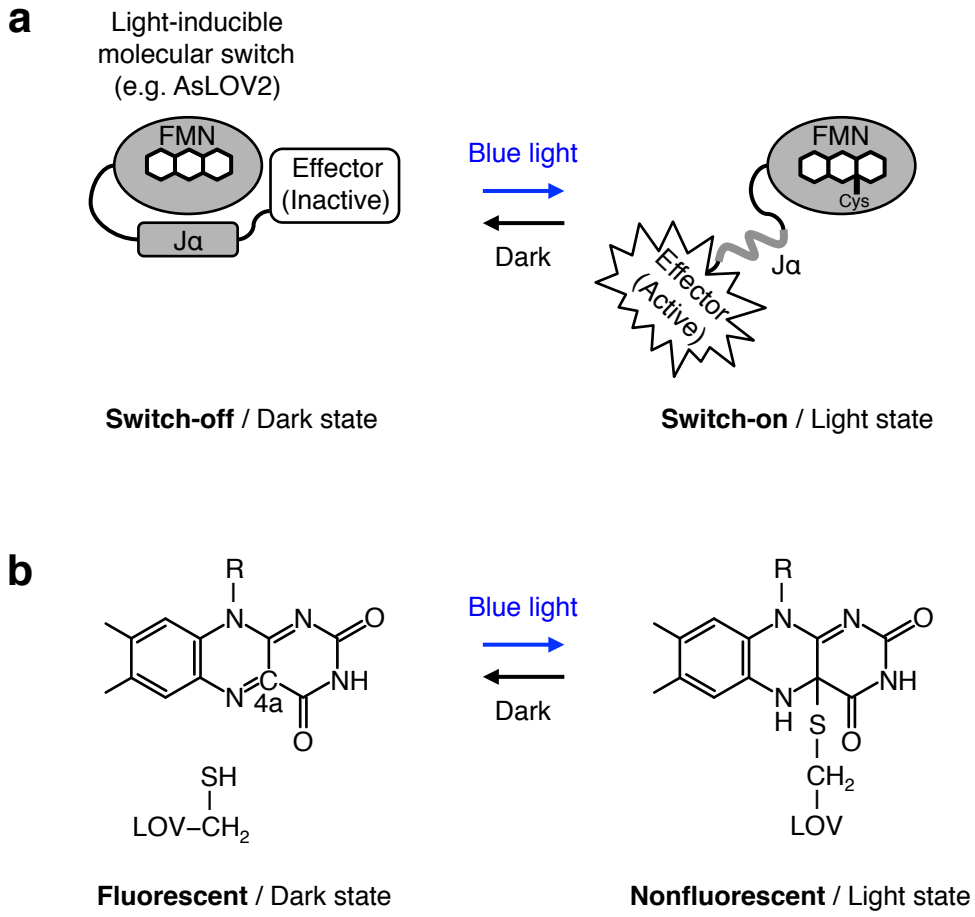

Figure 3-1. A LOV domain and its photocycle. (**a**) The second light-oxygen-voltage (LOV) domain derived from *Avena sativa* phototropin 1 (AsLOV2) binds a flavin cofactor (FMN) to sense blue light. In the dark state, the C-terminal Jα helix of AsLOV2 is tightly bound to its core domain (switch-off, left panel). Upon irradiation with blue light, the Jα helix is released from the core domain of AsLOV2 (switch-on, right panel). When the blue light is turned off, the open conformation of AsLOV2 in the light state is returned back to its closed conformation in the dark state (right to left). The blue light-dependent conformational change of AsLOV2 switches the activity of an effector domain, such as a protein with enzymatic activity and a peptide, connected at the C-terminus of AsLOV2. (**b**) A photochemical reaction, known as a photocycle, occurring between a LOV domain and a flavin cofactor. Blue light irradiation induces the formation of a covalent bond between the thiol group of a cysteine within a LOV domain and the C4a position of the isoalloxazine ring of flavin (left to right). The photoadduct spontaneously breaks when the LOV domain is returned back to the dark condition (right to left). The photoadduct formation and its break lead to loss of fluorescence from the flavin cofactor and its recovery, respectively.

The switch-off kinetics of the photoswitching proteins depends on the kinetics of photochemical reactions, termed photocycles (**Figure 3-1a, b**). Among photosensory domains derived from photoreceptors that absorb blue light, light-oxygen-voltage (LOV) domains have been well characterized compared with others. LOV domains bind a flavin cofactor, that is, flavin mononucleotide (FMN) or flavin adenine dinucleotide (FAD)[8]. Blue light irradiation quickly induces covalent bond formation between the flavin cofactor and a cysteine residue from a LOV domain on a time scale of sub-microseconds[8] (**Figure 3-1b**, left to right). However, thermally controlled reversion of the flavin cofactor in the dark condition requires minutes to hours depending on species of LOV domains[2-4,6,9], indicating that the thermal reversion is the rate-determining step for the photocycle (**Figure 3-1b**, right to left).

Structural analysis of LOV domains has revealed that approximately 20 amino acid residues surround the isoallexazine ring of the flavin cofactor[6,10,11]. Based on the structural information, some of these amino acid residues surrounding the flavin cofactor have been applied to point-mutation studies to control the thermal reversion of the cofactor. As a result, some variants of which thermal reversion rates are increased or decreased have been isolated so far[11-14]. Considering successful mutagenesis studies of a variety of fluorescent proteins[15-17], it is necessary to introduce multiple mutations simultaneously into LOV domains and conduct high-throughput screening of millions of candidates to further improve the thermal reversion kinetics. However, the previous approach is not easy to expand its experimental scale because it depends on absorption spectrophotometry for the evaluation of the variants.

Here I focus on a fluorescence property of the flavin cofactor to establish the present imaging-based high-throughput screening system that allows efficient tuning of the thermal reversion kinetics of LOV domains (**Figure 3-2**). Previous studies have revealed that the flavin cofactor within LOV domains emits green fluorescence in the dark state[18,19] (**Figure 3-1b**, left) and loses its fluorescence upon blue light irradiation due to the photoadduct formation[19] (**Figure 3-1b**, right). The cofactor has also been revealed to recover its fluorescence as a result of the thermal reversion[19] (**Figure 3-1b**, left). The present screening system is based on direct imaging of the thermal reversion process of the flavin cofactor (**Figure 3-2**). The imaging-based screening is conducted under a stereoscopic fluorescence microscope. In particular, I induced the photoadduct formation upon pulsed irradiation with intense blue light at 10 mW/cm^2. I also devised the imaging condition of the flavin cofactor not to induce re-formation of the photoadduct during the imaging of the thermal reversion process. I combine the fluorescence imaging of the thermal reversion kinetics with bacterial colonies-based conventional expression cloning technologies, which have previously been performed for altering photochemical properties of fluorescent proteins and LOV proteins[12,20]. To facilitate the screening, the temperature of agar plates is controlled. Based on the present imaging-based high-throughput screening system, I perform multi site-directed random mutagenesis of the second LOV domain derived from *Avena sativa* phototropin 1 (AsLOV2) and pick up AsLOV2 variants having improved thermal reversion kinetics from the mutant library (**Figure 3-2**).

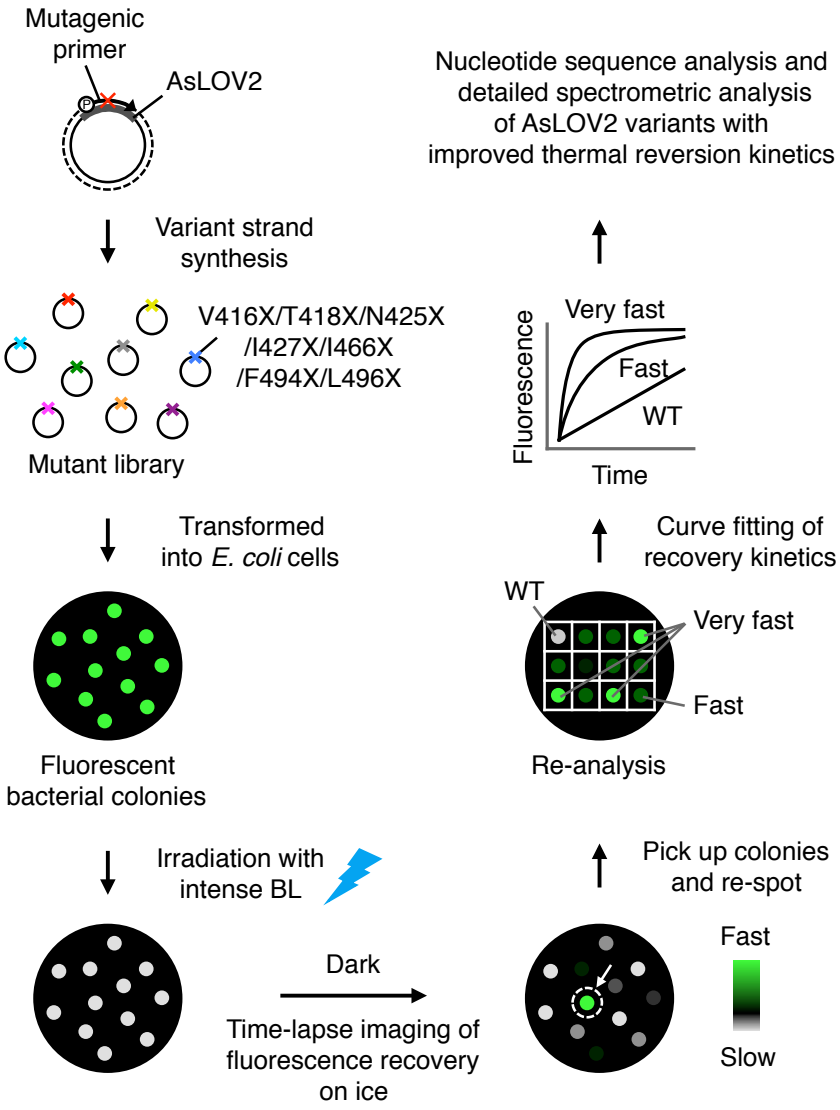

Figure 3-2. Imaging-based high-throughput system for tuning LOV domains. A library of cDNAs encoding AsLOV2 variants is generated using multi site-directed random mutagenesis. Mutagenic primers are designed to change codons encoding Val416, Thr418, Asn425, Ile427, Ile466, Phe494 and Leu496 of AsLOV2, which surround the isoalloxazine ring of the flavin cofactor. Bacterial colonies expressing AsLOV2 variants emit green fluorescence on an agar plate upon excitation at 480/40 nm. To facilitate screening of rapidly recovered fluorescent colonies, the agar plates where the transformed cells are seeded were cooled down on ice (or heated up 50 °C for screening of slowly recovered fluorescent colonies). Upon irradiation with blue light, the fluorescence of bacteria colonies quickly disappears. When the agar plates are returned back to the dark condition, the fluorescence is recovered. Time-lapse imaging of the fluorescence recovery pinpoints colonies expressing

AsLOV2 variants with improved thermal reversion kinetics. Fluorescent colonies showing rapid recovery are picked up and re-spotted on agar plates to conduct re-analysis. Following the screening and cloning, nucleotide sequence analysis and detailed spectrometric analysis of AsLOV2 variants with improved thermal reversion kinetics are conduced.

3-2. Experimental Section

3-2-1. Plasmid construction.

AsLOV2 used in the present study is the LOV2 domain derived from *Avena sativa* phototropin 1 (phototropin $1_{404\text{-}560}$) (accession number: O49003). Synthesized cDNA encoding the wild-type AsLOV2 with mammalian codons was obtained from GenScript (Piscataway, NJ, USA), and subcloned into a bacterial expression vector pCold I DNA (Takara, Tokyo, Japan) at *Hin*dIII and *Xba*I sites.

3-2-2. Protein expression and purification.

Wild-type AsLOV2 and its two variants, AsLOV2-V416T and AsLOV2-V416L, with an N-terminal six-residue histidine tag were expressed in *Escherichia coli* DH5α cells with the pCold I vector and cultured in 500 mL of a LB medium containing 100 μg/ml of ampicillin. The bacterial cells were grown at 37 °C until they reached a density of approximately OD_{600} = 0.5. Protein expression was induced by addition of isopropyl β-D-thiogalactoside (IPTG) at a final concentration of 0.1 mM following a temperature downshift from 37 to 15 °C. The bacterial cells were cultured for 24 h following the induction and lysed by sonication. The histidine-tagged proteins were purified by TALON resin chromatography (Clontech, Palo Alto, CA). These protein samples were eluted with an imidazole solution (500 mM imidazole, 50 mM sodium phosphate, 300 mM NaCl, pH 7.0) and dialyzed against a solution (pH 7.5) containing 50 mM Tris HCl and 150 mM NaCl for 24 h. The samples were concentrated with an Amicon Ultra centrifugal filter device (Millipore, Bedford, MA, USA). Protein concentrations were determined by the Bradford method (Bio-Rad, Hercules, CA,

USA) using BSA as a standard.

3-2-3. Spectral analysis.

Absorption spectrometry was performed at room temperature using an Evolution Array spectrophotometer (Thermo Scientific, Waltham, MA, USA), which equips arrayed detectors for the simultaneous acquisition of full-spectrum data without scanning. Fluorescence spectra of wild-type AsLOV2 were determined at room temperature using an F-7000 spectrofluorometer (Hitachi High-Technologies, Tokyo, Japan). Fluorescence quantum yields (ϕ) of wild-type AsLOV2, AsLOV2-V416T and AsLOV2-V416L were determined at room temperature using an absolute quantum yield measurement system (Quantaurus-QY C11347-01, Hamamatsu Photonics, Hamamatsu, Japan).

3-2-4. Multi site-directed random mutagenesis.

I performed site-directed random mutagenesis of seven amino acid residues of AsLOV2, Val416, Thr418, Asn425, Ile427, Ile466, Phe494 and Leu496, using Multi Site-Directed Mutagenesis Kit (MLB, Nagoya, Aichi, Japan)[15] according to the manufacturer's instructions. Among the seven residues, I first introduced mutations into three residues, Asn425, Ile427 and Ile466. Sequences for two degenerative primers for the mutation of the three residues are shown as follows: Primer-1 for the mutation of Asn425 and Ile427, 5'-CCTAGACTGCCCGACNNNCCTNNNATTTTCGCATCTGAT-3'; Primer-2 for the mutation of Ile466,

5’-GCAACCGTGAGGAAGNNNCGCGACGCCATTGAT-3’. Next I introduced mutations into four amino acid residues, Val416, Thr418, Phe494 and Leu496. Sequences for two degenerative primers for the mutation of the four amino acid residues are shown as follows: Primer-3 for the mutation of Val416 and Thr418, 5’-ATTGAAAAGAACTTCNNNATTNNNGACCCTAGACTGCCC-3’; Primer-4 for the mutation of Phe494 and Leu496, 5’-AAATTCTGGAACCTGNNNCACNNNCAGCCTATGAGGGAC-3’.

3-2-5. Imaging-based screening system.

E. coli DH5α cells were transformed with plasmids respectively encoding AsLOV2 and its variants, and seeded on LB agar media plates containing 100 μg/mL ampicillin and 10 μM IPTG, which was optimized for the growth of *E. coli* cells on agar media and protein expression. The cells were grown at 37 °C for 16 h. Protein expression was induced by a temperature downshift from 37 to 15 °C. The cells were incubated in the dark condition at 15 °C for 48 h following the induction. Bacterial colonies grown on agar plates were imaged on an M205 FA epifluorescence microscope (Leica, Wetzlar, Germany) equipped with a Retiga 1300i digital camera (Qimaging, Burnaby, BC, Canada). The system was controlled by MetaMorph software (Molecular Devices, Union City, CA, USA). For the fluorescence imaging, the agar plates were excited at 480/40 nm for 500 ms with 30 % FIM. Images were obtained through a barrier long pass filter LP 510 nm. To facilitate the screening, all the bacterial colonies expressing AsLOV2 variants on agar plates were chilled on ice for 10 min or heated up at 50 °C for 5 min using a heat block in the dark prior to imaging.

3-2-6. Light source.

Blue light irradiation of all the samples, such as purified proteins and bacterial colonies on agar plates, was performed with a LED light source (470 nm, CCS Inc., Kyoto, Japan) for 10 s at 10 mW/cm^2.

3-2-7. Curve fitting.

I fitted all the recovery curves of absorption and fluorescence of purified AsLOV2 and its variants to the following single exponential equation using the online curve-fitting tool at http://zunzun.com: $Y = A\{1 - \exp(-kt)\} + B$, where Y represents an absorbance or fluorescence intensity at time t, A and B are parameters, and k represents the rate constant. Time constant τ was determined using the following equation: $\tau = 1/k$.

Time course of a fluorescence intensity change of each bacterial colony after irradiation with blue light was plotted with a normalized intensity calculated as follow: Normalized intensity = $(I - I_{after})/(I_{before} - I_{after})$, where I represents a fluorescence intensity at different time points after irradiation with blue light, I_{after} represents a fluorescence intensity just after irradiation with blue light, and I_{before} represents a fluorescence intensity just before the irradiation. All the recovery curves of the normalized intensities were fit well with the following single exponential equation: $Y = A\{1 - \exp(-kt)\}$, where Y represents the normalized intensity at time t, A is a parameter, and k represent the rate constant. Half-recovery time $t_{1/2}$ was determined using the following equation: $t_{1/2} = \ln 2/k$.

3-3. Results

3-3-1. Fluorescence imaging of thermal reversion of AsLOV2 expressed in bacterial colonies.

AsLOV2 is a photosensory domain that binds with FMN as a cofactor[18]. For the spectral analysis of wild-type AsLOV2, I first investigated absorption spectrum of its purified protein. AsLOV2 exhibited major absorption at 428, 447 and 474 nm in the dark condition (**Figure 3-3a**), while upon irradiation with blue light (470 nm, 10 mW/cm^2, 10 s), the major absorption peaks immediately disappeared[2,3] (**Figure 3-3a**). The major absorption peaks of AsLOV2 were gradually recovered when the sample was returned back to the dark condition[2,3] (**Figure 3-3b**). The recovery of the absorption at 447 nm was fit well with a single exponential function (**Figure 3-3c**). I calculated a time constant τ of 55 s (rate constant = 1.8×10^{-2}). The result is consistent with several previous reports (τ = approximately 60 ~ 80 s)[3,13].

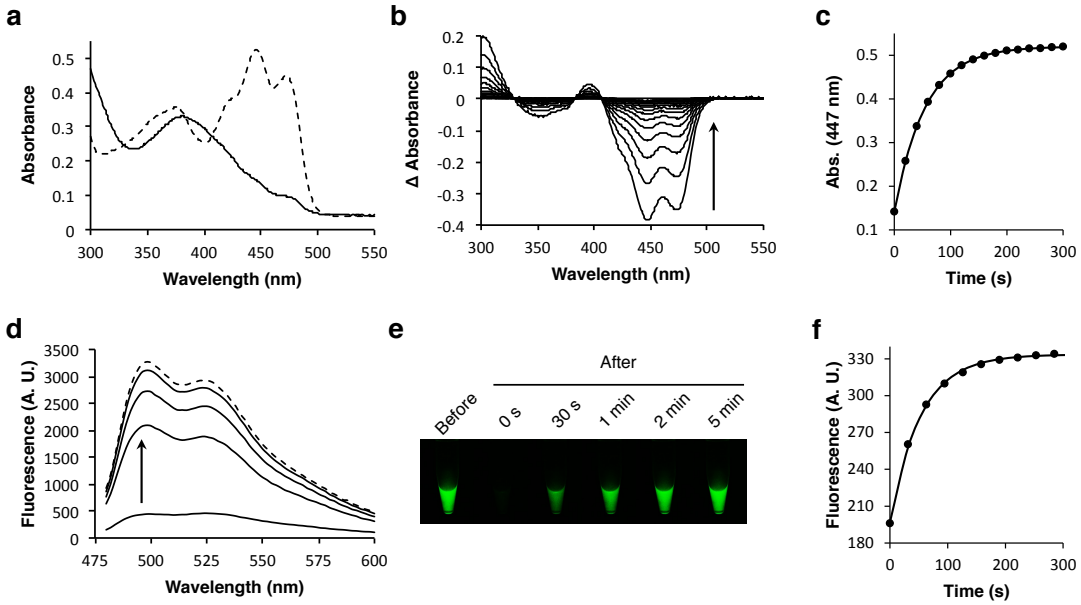

Figure 3-3. Spectral characterization of wild-type AsLOV2. (**a**) Absorption spectra of purified wild-type AsLOV2 protein before (dashed line) and after (solid line) irradiation with blue light. (**b**) Absorption difference spectra of purified wild-type AsLOV2 protein after irradiation with blue light. Δ Absorbance is calculated by subtracting absorbance before irradiation with blue light from that at different time points after the irradiation. Spectra were recorded every 20 s. Arrow indicates spectral changes with time. (**c**) Recovery of absorption at 447 nm shown in Figure 3-3b. The absorption recovery was fit with a single exponential curve with a time constant of 55 s (solid line). (**d**) Fluorescence spectra of purified wild-type AsLOV2 protein upon excitation with 450 nm before (dashed line) and after (solid lines) irradiation with blue light. Arrow indicates spectral changes with time. (**e**) Time-lapse of fluorescence images of purified wild-type AsLOV2 protein. AsLOV2 emitted strong green fluorescence upon excitation at 480/40 nm for 500 ms with 30 % FIM. The images were obtained with a stereoscopic fluorescence microscope through a long pass filter (~ 510 nm cutoff). The sample is collected in a 1.5 mL microtube. (**f**) Time course of the fluorescence recovery of purified AsLOV2 protein. Fluorescence change was recorded every 30 s. The fluorescence recovery was fit with a single exponential curve with a time constant of 54 s (solid line). Purified wild-type AsLOV2 protein was concentrated to 1.9 mg/ml for all the spectral characterizations.

I next examined the fluorescence property of wild-type AsLOV2 to investigate whether fluorescence recovery kinetics is consistent with the recovery kinetics of absorption. Spectral analysis of purified AsLOV2 protein showed that the photosensory domain emitted fluorescence with double peaks at 498 and 522 nm in the dark state[19] (**Figure 3-3d**). The fluorescence of AsLOV2 quickly disappeared upon irradiation with blue light at 10 mW/cm^2 (Ref. 19) (**Figure 3-3d**). When the sample was returned back to the dark condition, gradual recovery of the fluorescence spectra was observed[19] (**Figure 3-3d**).

I further examined time-lapse imaging of the fluorescence recovery of purified AsLOV2 protein under a stereoscopic fluorescence microscope equipped with a CCD camera (**Figure 3-3e**). The fluorescence recovery at 498 nm was fit well with a single exponential function (**Figure 3-3f**). Its time constant τ was 54 s (rate constant = 1.9×10^{-2}), consistent with the time constant of the absorption recovery at 447 nm. The result indicates that the time-lapse imaging of fluorescence recovery of AsLOV2 can be an alternative to the conventional approach based on absorption spectrophotometry to monitoring the thermal reversion of the flavin cofactor from its photoadduct.

I show that the time-lapse imaging of fluorescence recovery of AsLOV2 can be combined with a bacterial colonies-based expression cloning technique. *E. coli* cells were transformed with a plasmid encoding wild-type AsLOV2, and then seeded onto agar media plates to give a density of 800 ~ 1,000 colonies per plate. Green fluorescence was observed from the bacterial colonies expressing AsLOV2 upon excitation at 480/40 nm (**Figure 3-4a**). The fluorescence level was much

stronger than autofluorescence of bacterial cells and that of the agar plate (data not shown). The green fluorescence of the bacterial colonies immediately disappeared upon irradiation with blue light at 10 mW/cm^2, and then recovered to the initial level in 3 minutes when the agar plate was returned back to the dark condition. The fluorescence recovery kinetics was not affected by the colony size (**Figure 3-4b, c**). The result indicates that the present imaging-based system is applicable to efficient and precise investigation of the thermal reversion kinetics of AsLOV2.

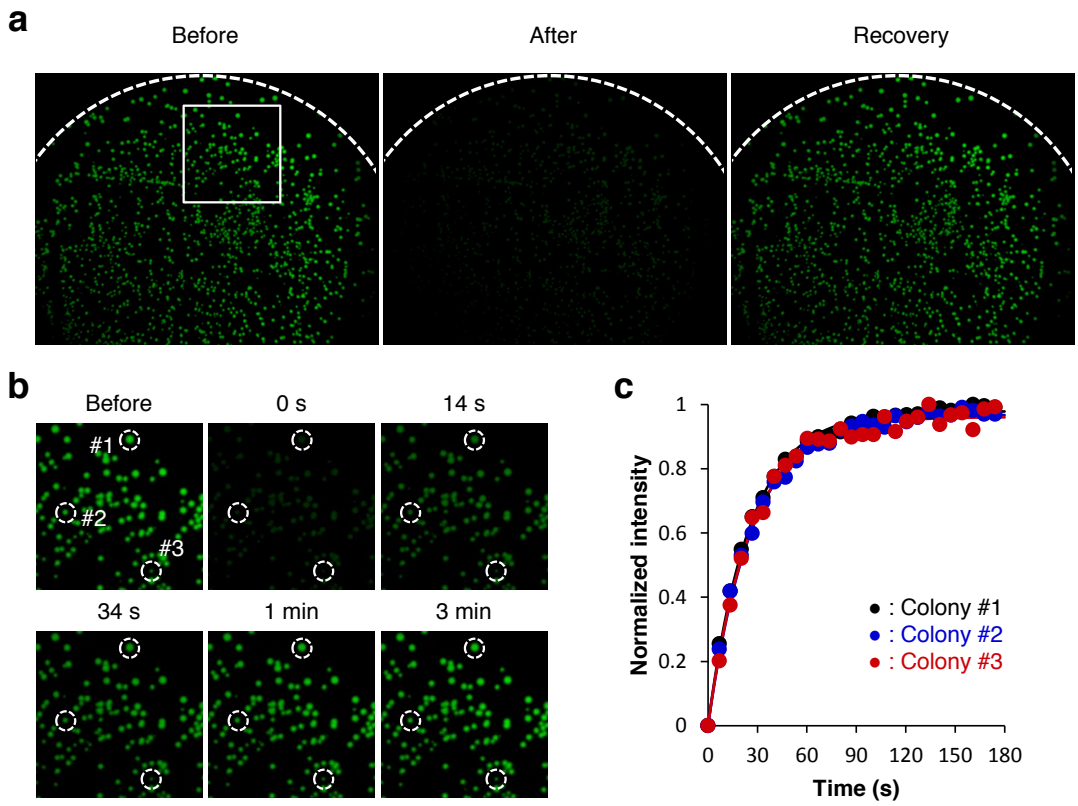

Figure 3-4. Direct imaging of the thermal reversion of wild-type AsLOV2. (**a**) Bacterial colonies expressing wild-type AsLOV2 on an agar plate were irradiated with blue light, and fluorescence recovery of its flavin cofactor was visualized with a stereoscopic fluorescence microscope. (**b**) Time-lapse imaging of the fluorescence recovery of wild-type AsLOV2 after irradiation with blue light. The region boxed with a white square in Figure 3-4a are magnified. (**c**) Time course of the fluorescence recovery of three independent bacterial colonies shown in Figure 3-4b with white dashed circles. The fluorescence recovery was fit with single exponential curves (solid lines).

3-3-2. Development of fast-cycling AsLOV2 variants

Next I perform multi site-directed mutagenesis of AsLOV2 and employ the present imaging-based system for high-throughput screening and cloning of AsLOV2 variants having fast thermal reversion kinetics. The flavin cofactor of AsLOV2 is surrounded by approximately 20 amino acid residues[10]. Among them, I selected seven amino acid residues, Val416, Thr418, Asn425, Ile427, Ile466, Phe494 and Leu496, on the basis of previous mutagenesis studies of several LOV domains, in which various mutants with altered thermal reversion kinetics had been reported (**Figure 3-5**)[11-13]. Multi site-directed mutagenesis was conducted on the seven amino acid residues. Based on nucleotide sequence analysis, I confirmed that all the codons encoding the seven amino acid residues were randomly mutated as expected. Bacterial cells were transformed with the mutagenized plasmids and then seeded onto agar plates to give a density of 800 ~ 1,000 colonies per plate. In addition, because the thermal reversion was more decelerated at lower temperature (**Figure 3-6a**), the agar plates were cooled down on ice in the dark prior to imaging. This was beneficial to efficiently separate variants of which thermal reversion kinetics exhibited only subtle difference between them at room temperature.

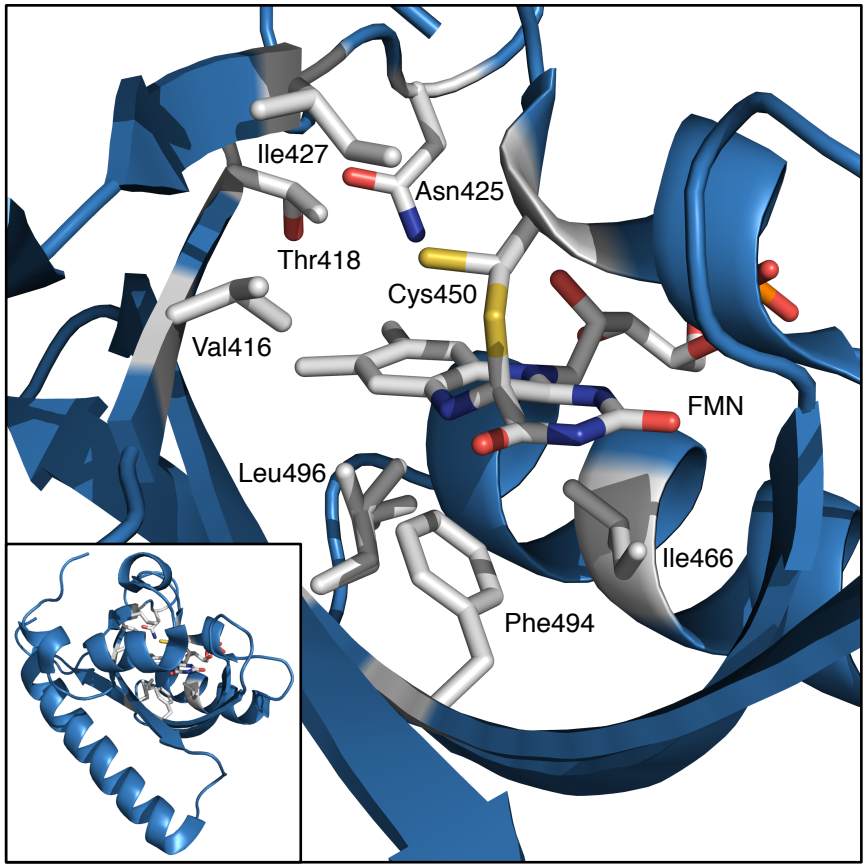

Figure 3-5. Crystal structure of wilt-type AsLOV2 in the light state. Structural analysis of wild-type AsLOV2 (PDB: 2V1B) has previously revealed that approximately 20 amino acid residues surround the isoallexazine ring of FMN. Among them, seven amino acid residues, Val416, Thr418, Asn425, Ile427, Ile466, Phe494 and Leu496, represented by stick model, were selected for the present mutagenesis study. The crystal structure shows the formation of the covalent bond between Cys450 and FMN in the light state. Two alternative side chain conformations, dark conformation and light conformation, of Cys450 are shown in the structure because dark conformation is present in the light state structure at 10% occupancy. Inset shows an overview of AsLOV2 structure.

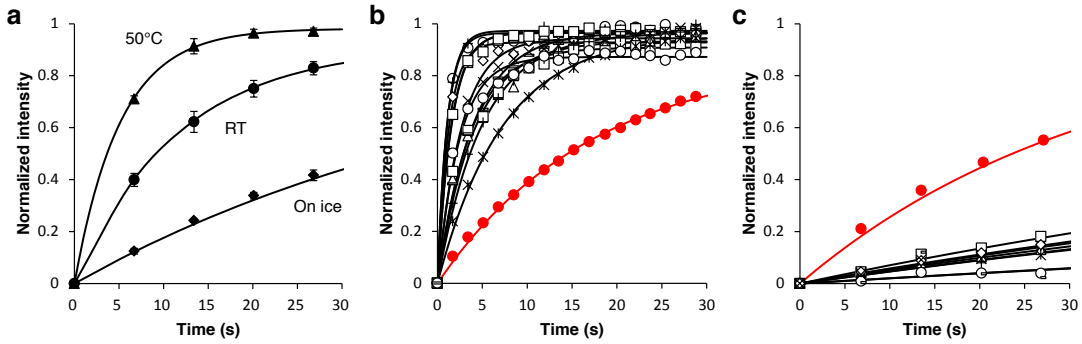

Figure 3-6. Mutagenesis and screening of AsLOV2 variants with improved thermal reversion kinetics. (**a**) Fluorescence recovery of wild-type AsLOV2 after irradiation with blue light at room temperature (closed circle), at 50 °C (closed triangle), and on ice (closed diamond). The results are means ± S.D. of three independent measurements. (**b**) Time course of fluorescence recovery of wild-type AsLOV2 (red) and that of AsLOV2 variants with fast thermal reversion kinetics (black). Twelve different fast variants obtained in the present partial screening are shown. Fluorescence intensity was recorded every 1.7 s at room temperature. (**c**) Time course of fluorescence recovery of wild-type AsLOV2 (red) and that of AsLOV2 variants with slow thermal reversion kinetics (black). Eight different slow variants obtained in the present partial screening are shown. Fluorescence intensity was recorded every 6.8 s at room temperature. Wild-type AsLOV2 and its variants were expressed in bacterial cells and imaged with a stereoscopic fluorescence microscope on an agar plate (a, b and c). The fluorescence recovery was fit with single exponential curves (a, b and c).

I observed more than 20,000 colonies expressing AsLOV2 variants and picked up 26 colonies showing substantially accelerated thermal reversion kinetics on ice. The colonies were re-spotted on agar plates and then confirmed that they exhibited substantially faster kinetics than wild-type AsLOV2 at 25 °C (**Figure 3-6b**). Nucleotide sequence analysis revealed that 12 different variants were included in the 26 clones (**Table 3-1**). Among them, four AsLOV2 variants respectively having substitution of V416T, N425Q/I427V, N425S/I427L/I466M and V416T/T418S exhibited particularly faster thermal reversion kinetics than others (**Table 3-1**).

Table 3-1. Screening of rapidly- or slowly-recovered fluorescent colonies expressing AsLOV2 variants.

Variants	Frequency	Half-recovery time $t_{1/2}$ (s)
V416T	5/26	0.75
N425Q/I427V	8/26	0.75
N425S/I427L/I466M	1/26	0.85
V416T/T418S	4/26	1.1
T418S	1/26	1.1
N425H/I427L/I466M	1/26	1.7
I427C	1/26	1.8
N425H/I427L/I466V	1/26	2.5
N425S	1/26	2.8
N425Q/I427L	1/26	2.8
I427V	1/26	3.5
N425Q	1/26	5.0
F494T/L496C	1/9	0.75×10^2
V416I	1/9	0.85×10^2
F494I	2/9	0.89×10^2
F494I/L496C	1/9	0.90×10^2
V416I/T418A	1/9	1.0×10^2
F494I/L496S	1/9	1.1×10^2
V416C/T418P/N425P/I466V/F494K	1/9	1.6×10^2
V416L	1/9	1.6×10^2

I purified the AsLOV2-V416T protein, one of the fastest variants, and conducted its kinetic analysis at room temperature upon blue light irradiation by monitoring absorption at 447 nm. AsLOV2-V416T was found to exhibit thermal reversion with a time constant τ of 2.6 s (rate constant = 3.8×10^{-1}), 21-fold faster than wild-type AsLOV2 (**Figure 3-7a**, **Table 3-2**). In addition, the present variant is faster than any other variants, such as AsLOV2-I427V (τ = 4 s), reported to exhibit improved thermal reversion kinetics so far (**Table 3-2**)[12]. Different from the case of thermal reversion kinetics, I observed no significant difference in fluorescence quantum yield between AsLOV2-V416T (ϕ = 0.14) and wild-type AsLOV2 (ϕ = 0.13).

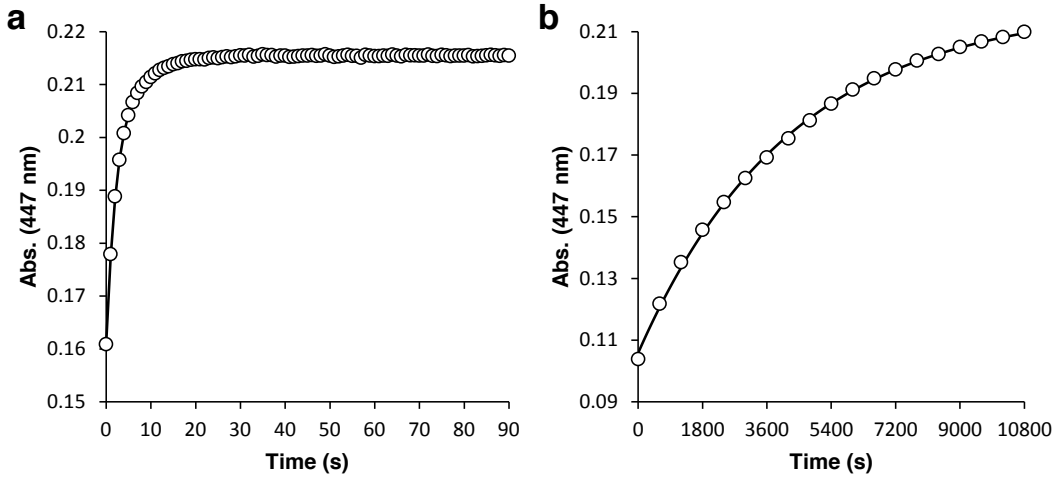

Figure 3-7. Thermal reversion kinetics of AsLOV2-V416T and AsLOV2-V416L. (**a**) Thermal reversion kinetics of purified AsLOV2-V416T protein at room temperature. The absorption at 447 nm was recorded every 1.0 s after irradiation with blue light and fit with a single exponential curve with a time constant τ of 2.6 s. (**b**) Thermal reversion kinetics of purified AsLOV2-V416L protein at room temperature. The absorption at 447 nm was recorded every 60 s after irradiation with blue light and fit with a single exponential curve with a time constant τ of 4.3×10^3 s.

Table 3-2. Parameters for recovery kinetic in AsLOV2 variants.

Variants	Time constant τ (s)	Rate constant (s^{-1})	Reference
WT	55	1.8×10^{-2}	This study
V416T	2.6	3.8×10^{-1}	This study
I427V	4	NA	12
V416I/L496I	1.0×10^{3}	9.9×10^{-4}	13
V416L	4.3×10^{3}	2.4×10^{-4}	This study

NA, not available.

Given the possibility that mutagenesis of the seven positions produces 1.28 $\times 10^9$ different variants, the present screening of 2×10^4 colonies is insufficient to cover all the variants. Despite the partial screening, I have obtained faster variants than existing ones. Further scaled-up screening may lead to identification of substantially faster AsLOV2 variants than those obtained in the present partial screening.

3-3-3. Slow-cycling AsLOV2 variants.

Next I show that the present imaging-based high-throughput screening system provide a powerful tool not only for fast-cycling variants but also for variants with substantially slower kinetics than wild-type AsLOV2. As in the case of the fast-cycling variants, multi site-directed random mutagenesis was conducted to the seven amino acid residues, Val416, Thr418, Asn425, Ile427, Ile466, Phe494 and Leu496, surrounding the flavin cofactor of AsLOV2. Contrary to the case of fast-cycling variants, the agar plates were heated up to 50 °C in the dark prior to imaging to accelerate the screening of AsLOV2 variants with substantially decelerated thermal reversion kinetics at room temperature (**Figure 3-6a**). I found no significant side effect of the treatment at 50 °C on bacterial culture after the screening.

As a result of screening of more than 20,000 colonies, I picked up 9 colonies showing substantially decelerated thermal reversion kinetics at 50 °C. The colonies were re-spotted on agar plates and then confirmed that they exhibited substantially slower kinetics than wild-type AsLOV2 at 25 °C (**Figure 3-6c**).

Nucleotide sequence analysis identified 8 different variants (**Table 3-1**). Among them, AsLOV2-V416L and AsLOV2-V416C/T418P/N425P/I466V/F494K exhibited particularly slower thermal reversion kinetics than others (**Table 3-1**). I purified the AsLOV2-V416L protein, one of the slowest variants, and conducted its kinetic analysis at room temperature upon blue light irradiation by monitoring absorption at 447 nm. AsLOV2-V416L was shown to exhibit thermal reversion with a time constant τ of 4.3×10^3 s, 78-fold slower than wild-type AsLOV2 (**Figure 3-7b**, **Table 3-2**). In addition, AsLOV2-V416L was 4.3-fold slower than the variant previously reported as the slowest one (AsLOV2-V416I/L496I, $\tau = 1.0 \times 10^3$ s) (**Table 3-2**). Using the purified proteins, I also show that AsLOV2-V416L has similar fluorescence quantum yield ($\phi = 0.11$) to wild-type AsLOV2 ($\phi = 0.13$).

3-4. Discussion

In the present study, I have developed a high-throughput screening system for tuning LOV domains. Its main point is that the screening system is based on time-lapse and direct imaging of fluorescence recovery of the flavin cofactor. This is what has allowed me to expand the experimental scale and conduct a high-throughput screening of gene library with multi site-directed random mutations under a stereoscopic fluorescence microscope. The temperature control was also devised to facilitate the screening of variants with improved thermal reversion kinetics. The present screening system was validated with AsLOV2, one of the most frequently used photoreceptors and photosensory domains for optogenetics[1].

According to structural studies of AsLOV2, its flavin cofactor is surrounded by approximately 20 amino acid residues. In the process of experimental design of the present multi site-directed mutagenesis of AsLOV2, I focused on Val416, Thr418, Asn425, Ile427, Ile466, Phe494 and Leu496. These seven amino acid residues were selected on the basis of previous studies on kinetic mutants of several LOV proteins. Among the seven amino acid residues, I am particularly paying attention to the amino acid residue 416. This is because I found that its single substitution was enough to generate the faster variant (AsLOV2-V416T) than any other variants reported so far. Furthermore, I also found that its single substitution also resulted in the generation of the slower variant (AsLOV2-V416L) than any other variants reported to date. The side chain of Val416 of AsLOV2 is located within 4Å of its Cys450 responsible for the photoadduct formation[10] (**Figure 3-8a**). On the basis of structural analysis of another LOV protein, known as Vivid (VVD), and its kinetic variants, Zoltowski *et al*.

have found that Ile74 of VVD, which is equivalent to Val416 in the case of AsLOV2, is one of critical amino acid residues affecting the thermal reversion kinetics of VVD[6,13]. They have reasoned that substitutions of Ile74 of VVD may affect conformation stability of its Cys108, which is equivalent to Cys450 of AsLOV2 (**Figure 3-8b,c**). This may lead to changing the steric stability of the adduct state and thereby result in acceleration of thermal reversion in the case of a variant (VVD-I74V) having faster thermal reversion kinetics than wild-type VVD. They also have proposed additional effects including an increase in solvent accessibility to the flavin and/or Cys108 on the I74V variant of VVD. However, the present threonine (T) and leucine (L) substitutions, found to substantially accelerate and decelerate the thermal reversion kinetics, respectively, have not yet been applied to Ile74 of VVD. If structures of AsLOV2-V416T and AsLOV2-V416L can be solved, molecular mechanisms about how these substitutions have accelerated and decelerated the thermal reversion kinetics of AsLOV2 may be uncovered.

As a result of the present partial screening, I have developed several AsLOV2 variants with fast thermal reversion kinetics. These fast-cycling variants may contribute to the improvement of the kinetic features of AsLOV2-based existing optogenetic tools, such as LovTAP, PA-Rac and TULIPs[21-25]. In addition to the fast-cycling variants, I also have developed variants with substantially slower thermal reversion kinetics than wild-type AsLOV2 and any other AsLOV2 variants reported so far. The slow-cycling variants only require one-shot irradiation, but not continuous irradiation, to continuously activate optogenetic tools. Consequently, some unwanted side effects caused by the continuous irradiation, such as

phototoxicity and unfocused activation due to the sample drift, are expected to become avoidable. The present slow-cycling variants may provide a powerful tool for optogenentic control of cellular processes that requires sustained activation, such as gene regulation.

My approach based on fluorescence imaging of the thermal reversion of the flavin cofactor is not limited to AsLOV2 but is generally applicable to a variety of blue light photoswitching proteins that bind with flavin cofactors, such as LOV domain-containing proteins and cryptochromes[26]. The present study may provide a new opportunity for the development of molecular tools for optogenetics and thereby having an impact on the emerging research field.

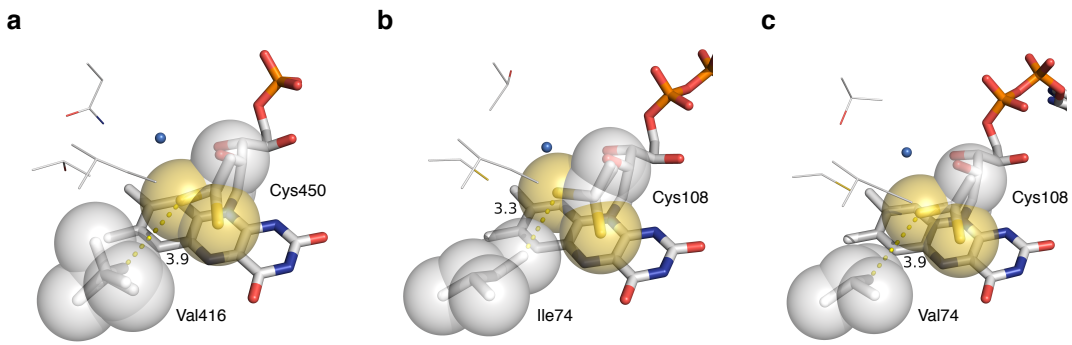

Figure 3-8. Structural analysis of Val416 of AsLO2 for thermal reversion. (**a**) A crystal structure of wild-type AsLOV2 in the dark state (PDB: 2V1A) shows the side chain of Val416 directed toward Cys450 (Ref. 10). The valine residue is located within 4Å of Cys450, but has no steric interaction with its side chain. (**b**) A crystal structure of wild-type VVD in the dark state (PDB: 2PD7) shows that Ile74, which is equivalent to Val416 of AsLOV2, positions its side chain in van der Waals contact with Cys108, which is equivalent to Cys450 of AsLOV2 (Ref. 6). Zoltowski *et al*. explain that the steric interaction of the methyl group may affect the conformation stability of Cys108 (Ref. 13). (**c**) A crystal structure of VVD-I74V in the dark state (PDB: 3HJK) shows that a valine substitution of Ile74 removes the methyl group of Ile74 from van der Waals area of Cys108 (Ref. 13). Key amino acid residues described above are represented by stick model and sphere model with a radius equal to the van del Waals surface. Other key amino acid residues, which are Thr418, Asn425 and Ile427 of wild-type AsLOV2 (a), and Cys76, Thr83 and Ile85 of wild-type VVD (b), and the VVD-I74V variant (c), for thermal reversion in LOV domains are represented by line model. Crystal structures of wild-type AsLOV2 (a), wild-type VVD (b) and the VVD-I74V variant (c) in the dark state show the amino acid residues located near the solvent channel (blue sphere).

3-5. References

1. Muller, K. & Weber, W. Optogenetic tools for mammalian systems. *Mol Biosyst* **9**, 596-608 (2013).
2. Salomon, M., Christie, J.M., Knieb, E., Lempert, U. & Briggs, W.R. Photochemical and mutational analysis of the FMN-binding domains of the plant blue light receptor, phototropin. *Biochemistry* **39**, 9401-10 (2000).
3. Swartz, T.E. et al. The photocycle of a flavin-binding domain of the blue light photoreceptor phototropin. *J Biol Chem* **276**, 36493-500 (2001).
4. Zikihara, K. et al. Photoreaction cycle of the light, oxygen, and voltage domain in FKF1 determined by low-temperature absorption spectroscopy. *Biochemistry* **45**, 10828-37 (2006).
5. Banerjee, R. et al. The signaling state of Arabidopsis cryptochrome 2 contains flavin semiquinone. *J Biol Chem* **282**, 14916-22 (2007).
6. Zoltowski, B.D. et al. Conformational switching in the fungal light sensor Vivid. *Science* **316**, 1054-7 (2007).
7. Toettcher, J.E., Voigt, C.A., Weiner, O.D. & Lim, W.A. The promise of optogenetics in cell biology: interrogating molecular circuits in space and time. *Nat Methods* **8**, 35-8 (2011).
8. Crosson, S., Rajagopal, S. & Moffat, K. The LOV domain family: photoresponsive signaling modules coupled to diverse output domains. *Biochemistry* **42**, 2-10 (2003).
9. Kottke, T., Heberle, J., Hehn, D., Dick, B. & Hegemann, P. Phot-LOV1: photocycle of a blue-light receptor domain from the green alga Chlamydomonas

reinhardtii. *Biophys J* **84**, 1192-201 (2003).

10. Halavaty, A.S. & Moffat, K. N- and C-terminal flanking regions modulate light-induced signal transduction in the LOV2 domain of the blue light sensor phototropin 1 from Avena sativa. *Biochemistry* **46**, 14001-9 (2007).
11. Mitra, D., Yang, X. & Moffat, K. Crystal structures of Aureochrome1 LOV suggest new design strategies for optogenetics. *Structure* **20**, 698-706 (2012).
12. Christie, J.M. et al. Steric interactions stabilize the signaling state of the LOV2 domain of phototropin 1. *Biochemistry* **46**, 9310-9 (2007).
13. Zoltowski, B.D., Vaccaro, B. & Crane, B.R. Mechanism-based tuning of a LOV domain photoreceptor. *Nat Chem Biol* **5**, 827-34 (2009).
14. Zayner, J.P., Antoniou, C. & Sosnick, T.R. The amino-terminal helix modulates light-activated conformational changes in AsLOV2. *J Mol Biol* **419**, 61-74 (2012).
15. Sawano, A. & Miyawaki, A. Directed evolution of green fluorescent protein by a new versatile PCR strategy for site-directed and semi-random mutagenesis. *Nucleic Acids Res* **28**, E78 (2000).
16. Shaner, N.C. et al. Improved monomeric red, orange and yellow fluorescent proteins derived from Discosoma sp. red fluorescent protein. *Nat Biotechnol* **22**, 1567-72 (2004).
17. Tsutsui, H., Karasawa, S., Shimizu, H., Nukina, N. & Miyawaki, A. Semi-rational engineering of a coral fluorescent protein into an efficient highlighter. *EMBO Rep* **6**, 233-8 (2005).
18. Christie, J.M., Salomon, M., Nozue, K., Wada, M. & Briggs, W.R. LOV (light,

oxygen, or voltage) domains of the blue-light photoreceptor phototropin (nph1): binding sites for the chromophore flavin mononucleotide. *Proc Natl Acad Sci U S A* **96**, 8779-83 (1999).

19. Kasahara, M. et al. Photochemical properties of the flavin mononucleotide-binding domains of the phototropins from *Arabidopsis*, rice, and *Chlamydomonas reinhardtii*. *Plant Physiol* **129**, 762-73 (2002).
20. Heim, R., Prasher, D.C. & Tsien, R.Y. Wavelength mutations and posttranslational autoxidation of green fluorescent protein. *Proc Natl Acad Sci U S A* **91**, 12501-4 (1994).
21. Strickland, D., Moffat, K. & Sosnick, T.R. Light-activated DNA binding in a designed allosteric protein. *Proc Natl Acad Sci U S A* **105**, 10709-14 (2008).
22. Wu, Y.I. et al. A genetically encoded photoactivatable Rac controls the motility of living cells. *Nature* **461**, 104-8 (2009).
23. Pham, E., Mills, E. & Truong, K. A synthetic photoactivated protein to generate local or global Ca(2+) signals. *Chem Biol* **18**, 880-90 (2011).
24. Strickland, D. et al. TULIPs: tunable, light-controlled interacting protein tags for cell biology. *Nat Methods* **9**, 379-84 (2012).
25. Lungu, O.I. et al. Designing photoswitchable peptides using the AsLOV2 domain. *Chem Biol* **19**, 507-17 (2012).
26. Zoltowski, B.D. & Gardner, K.H. Tripping the light fantastic: blue-light photoreceptors as examples of environmentally modulated protein-protein interactions. *Biochemistry* **50**, 4-16 (2011).

Chapter 4

General conclusion

In Chapter 2, I have developed pairs of two distinct photoswitching proteins based on re-engineering of the natural photoreceptor VVD derived from a filamentous fungus. This work was highly motivated by the fact that the nature of photoswitching proteins determines success or failure of optogenetic tools to control cellular signaling proteins and the related cellular functions. The present pairs of two distinct photoswitching proteins, named Magnet, were engineered to discriminate each other based on electrostatic interactions introduced into the dimer interface. This has successfully prevented homo-dimerization, which potentially could case serious technological problems, and selectively induced hetero-dimerization of the photoswitching proteins with light. Further mutagenesis has pinpointed a functional link between switch-off kinetics of the photoswitching proteins and its dimerization efficiency, and generated two types of contrasting variants: One with ~330-fold accelerated switchi-off kinetics but diminished dimerization efficiencies, and the other with ~15-fold enhanced dimerization efficiencies but slower switch-off kinetics. I have found a key engineering approach to solving the trade-off problem, and created the present photoswitching proteins having both substantially enhanced dimerization efficiencies and accelerated switch-off kinetics. I have demonstrated the capacity of Magnet by controlling a lipid kinase, protein kinase and small GTPases with highly spatiotemporal resolution. The present Magnet overcoming its inherent limitations provides a robust and versatile tool for optogenetic control of a wide variety of cellular signaling proteins and the related cellular functions.

In Chapter 3, I have developed high-throughput screening system to efficiently improve switch-off kinetics of blue light-absorbing natural photoreceptors. The

present approach is based on fluorescence imaging of thermal reversion of a flavin cofactor within blue light-absorbing photoreceptors. This is what has allowed to expand the experimental scale and to conduct a high throughput screening of gene library with multi site-directed random mutations under a stereoscopic fluorescence microscope. I have also devised temperature control to facilitate the screening of variants with improved switch-off kinetics. I have validated the present screening system with AsLOV2, one of the most frequently used photoreceptor for optogenetic tools and demonstrated that this approach allows to isolate AsLOV2 variants having substantially faster and slower switch-off kinetics, respectively. For example, AsLOV2-V416T exhibited thermal reversion with a time constant of 2.6 s, 21-fold faster than wild-type AsLOV2. I also have isolated AsLOV2-V416L that exhibited thermal reversion with a time constant of 4.3×10^3 s (78-fold slower than wild-type AsLOV2).

In addition to AsLOV2, the present approach to mutagenesis and high-throughput screening is applicable to a variety of blue light-absorbing photoreceptors, such as flavin-binding LOV proteins and cryptochromes. A future challenge of the present approach involves further improvement of Magnet to have much faster switch-off kinetics than the original one. The present, original Magnet described in Chapter 2 has switch-off kinetics of several tens of seconds. Considering from the fact that diffusion kinetics of biomolecules in cytosol is several tens micrometers per second, Magnet should be improved to have switch-off kinetics of a sub-second time scale. Magnet variants could be generated to have extremely fast switch-off kinetics based on the present mutagenesis and high-throughput

screening approach. Such photoswitching proteins generated by combining the ideas described in Chapters 2 and 3 should appear to offer a powerful tool to optically control the activity of signaling molecules with superior spatiotemporal precision at subcellular levels.

Multi-directional protein engineering study of naturally occurring photoreceptors described in this thesis provides a new opportunity for spatial and temporal control of protein activities and thereby contributes to the understanding and optical manipulation of a wide variety of cellular signaling processes.